Virginia Tech

School of Neuroscience

Summer Undergraduate Research Fellowship 2019

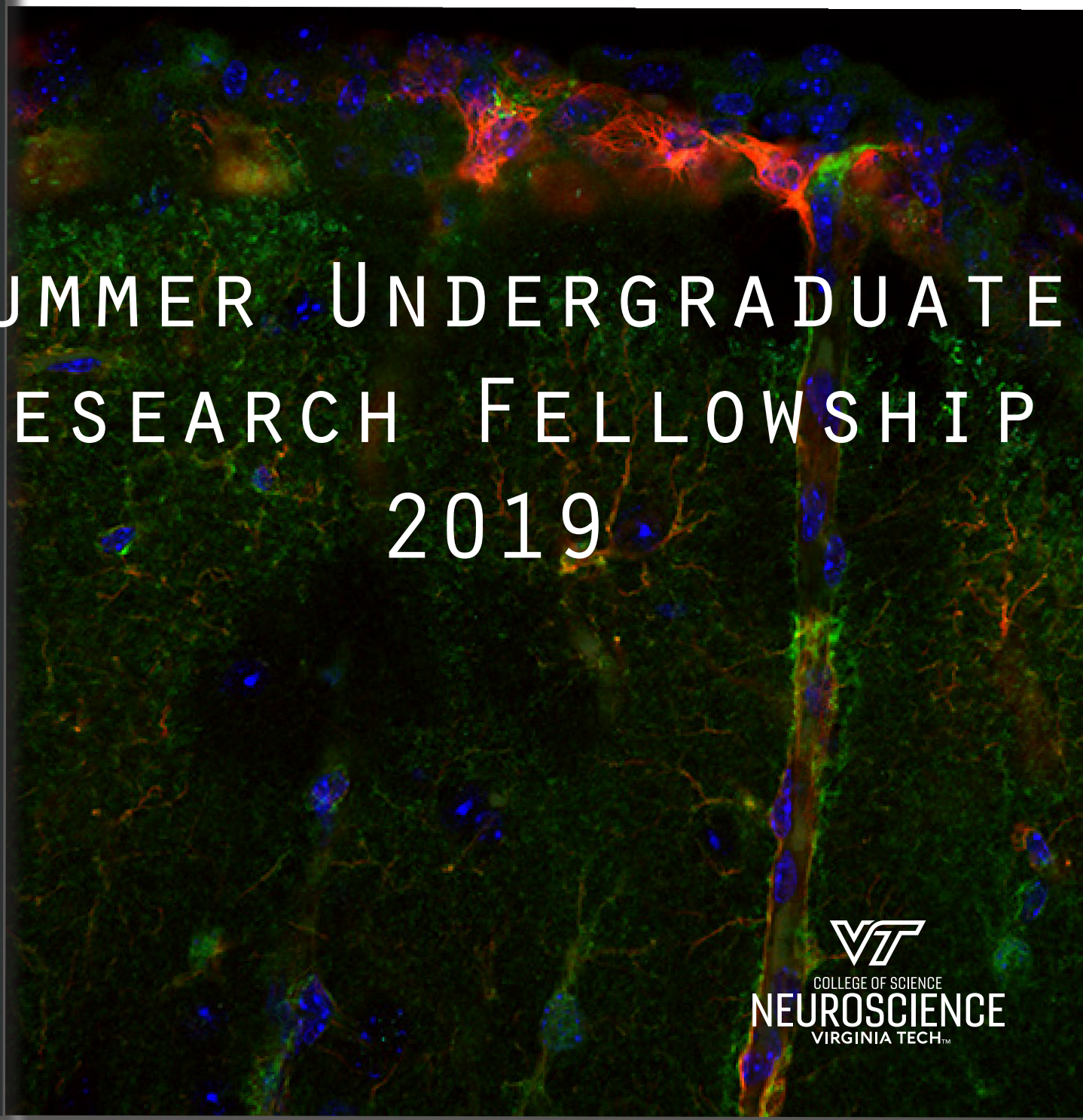

The Summer Undergraduate Research Fellowship in Neuroscience programs are paid summer internships that give students the opportunity to work within a neuroscience laboratory affiliated with the Virginia Tech School of Neuroscience.

The SURF-N program is an 11-week summer fellowship program, giving students the opportunity to experience a neuroscience laboratory, contribute to active research projects under the direction and leadership of School of Neuroscience faculty, and gain valuable experience in data presentation at the end of the summer. The expectation is that students will spend 40 hours per week immersed in a research environment assisting their faculty mentor in an ongoing research project. Students will be provided with real-world neuroscience research experience and bench skills beneficial to career development. The program concludes with a School of Neuroscience research retreat during which students are required to present their work.

This program was made possible by the generous support from: James and Lillian Gay foundation, EngelNovitt research fund, Gary Simonds research fund and the School of Neuroscience. The School of Neuroscience is grateful for providing our students with this life-changing opportunity.

Fellowship Recipients

Robert G. Bass
Mentor: Dr. Christopher K. Thompson
Equilin does not affect Thyroid Hormone Signaling in the Developing Xenopus laevis Tadpole Brain

Isiah J. Boyd
Mentor: Dr. Lina Nil
Nociceptive detection to electrophilic compounds requires TrpA1, but not painless, in Drosophila

Jack L. Browning
Mentor: Dr. Harald Sontheimer
Development of Perineuronal nets coincides with astrocytic maturation

Reagan Bullins
Mentor: Dr. Daniel English
Investigating the effects of single cell and network physiology on the performance of spike sorting methods

Gabe Coleman
Mentor: Dr. Alicia M. Pickrell
Monocyte specific EphA4: A Novel Regulator of Tissue Loss in the TBI Milieu

Deyton Cook
Mentor: Dr. Stefanie Robel
Astrocytes as Cellular Players in Maintaining the Blood-Brain Barrier

Failor Madison
Mentor: Dr. Mark Cline
Elucidating the hypothalamic mechanism of glucagon-like peptide 1-induced satiety

Jessica Maltman,
Mentor: Dr. Sarah Clinton
Implementing an Early-Life Stress Model that Uses a Limited Bedding Paradigm to Produce Fragmented and Unpredictable Maternal Care

Jamie Mustian
Mentor: Dr. Mike Bowers
A stuttering associated mutation in the gene Gnptab alters rat pup ultrasonic vocalizations

Giselle Nicole Rivero Ballon
Mentor: Dr. Georgia E. Hodes
Effect of Variable Stress on T Helper Cell Polarization

Sedovy MW
Mentor: Dr. Sarah Clinton
Altered Metabolic Activity and Hippocampal Changes in Stress Reactive Rats Exposed to Maternal Separation

Hannah G. Sturgeon
Mentor: Dr. Christopher K. Thompson
Reconstituted Mining Effluent Reduces Neuronal Proliferation in the Developing Brain and Slows Growth of Body Features in Wild-Caught Wood Frog Tadpoles

Rachael E. Ward
Mentor: Dr. John Chappell
Assessing Brain Microvasculature in a Model of Von Hippel-Lindau Mutations and the Potential Application of Ultrastructural Analysis

Lauren Weaver
Mentor: Dr. Mike Bowers
Neonatal overexpression of a truncated variant for Foxp1 alters ultrasonic vocalizations in rats

Jin Yoon
Mentor: Dr. Lina Ni
DOCC Function in Cool Avoidance in Drosophila Melanogaster Larvae

Equilin does not affect Thyroid Hormone Signaling in the Developing Xenopus laevis Tadpole Brain

Robert G. Bass III, Zahabiya Husain, Lara I. Dahora, Christopher K. Thompson

School of Neuroscience, Virginia Tech, Blacksburg VA

Abstract

Toxcast/Tox211 is a federally run research effort dedicated to better understanding the potential toxicity of thousands of chemicals in a high throughput manner. Among this list of compounds is equilin, an estrogen-like compound that was flagged as a potential thyroid hormone agonist. Here, we examine if equilin acts like a thyroid hormone agonist on cellular and molecular mechanisms of brain development in Xenopus laevis tadpoles. To examine the effect of equilin, tadpoles were divided into eight groups: 1 µL, 10 µL, and 100 µL of equilin; 1 µL, 10µM, and 100 µM of 17-β estradiol as an estrogen control; 15 µg/mL thyroxine (T4) as a thyroid hormone control; and a no-exposure control. After 4 days of treatment, animals were euthanized in MS-222. After fixation, body length was measured, and the brains dissected out. IHC was performed on brains labeling proliferating neural progenitor cells. Brains were then whole-mounted and analyzed using confocal microscopy. We found that equilin did not increase the number of dividing progenitor cells in a T4-like manner. Instead, equilin decreased proliferation in a dose-dependent manner, as did estradiol. In another experiment, RNA was extracted from tadpoles in each group and qPCR was performed, finding that equilin did not alter expression of thyroid hormone-sensitive genes. Our data indicate that equilin does not act as a thyroid hormone agonist in the Xenopus laevis nervous system but instead acts similarly to estradiol. Our data strongly suggest that equilin is not a TH disruptor, contrary to the findings of the ToxCast/Tox21 dataset.

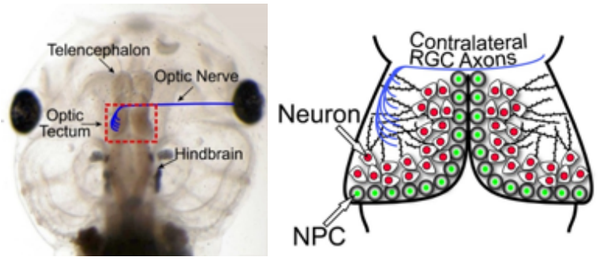

A) Dorsal aspect of the head of a Xenopus laevis tadpole. B) A schematic diagram of the midbrain area in the red box in A illustrating the retino-tectal circuit. Neural progenitor cells (NPC, green) are found in the ventricular proliferative zone. Neurons (red) are generated from NPCs. They extend dendrites (black) into the neuropil where they form synapses with other tectal neurons and/or RGC axons (blue).

Methods

Animals: Xenopus laevis albino tadpoles NF stage 46-47 (7-10 days old).

Hormone and disruptor treatment: Thyroxine (T4) was dissolved in 50mM NaOH, then diluted in Steinbergs rearing solution to working strength concentration (19 nM). 100 mg of Equilin was diluted in 3.72 ml DMSO. 200 ul of stock solution was diluted into 200 ml of Steinbergs to make a 100uM secondary stock. Working strength was made by diluting that solution 1:10, and 1:100 in Steinbergs. Groups of tadpoles were reared in 200ml of solution for up to four days.

Sacrifice and tissue processing: Tadpoles were killed on Day 4 with an overdose of MS222, and for IHC experiments were fixed overnight in 4%PFA.

Standard immunohistochemistry methods were used to stain whole-mount brains for CldU (Sigma, 1:1000) and Sytox-O (Life Sciences, 1:500).

Imaging and analysis: PFA-fixed brains were imaged on a Leica SP8 confocal microscope, and images were analyzed with Imaris and ImageJ.

QPCR: Brains were dissected into Trizol for mRNA extraction. Amount of mRNA was measured on a Nanodrop spectrophotometer. mRNA was converted to cDNA via iScript (Bio-Rad), and QPCR was done on a CFX384 RT-thermocycler using iTaq Universal QPCR mix. Reference genes were rps13 and rpl32. Change in expression was calculated using ΔΔCt.

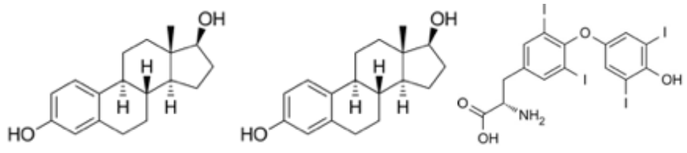

EQUILIN *17β-ESTRADIOL* *THYROXIN*

Equilin treatment induces distinct morphological head changes, but does not affect body length relative to CNTL

Figure 1) Images of tadpoles after 4 days with distinct alterations in facial morphology. Tadpoles exposed to equilin had their facial features severely altered. Tadpoles exposed to thyroid hormone also have changes in facial morphology, however the changes are dissimilar to those of estradiol, and typically require 7 days to fully develop.

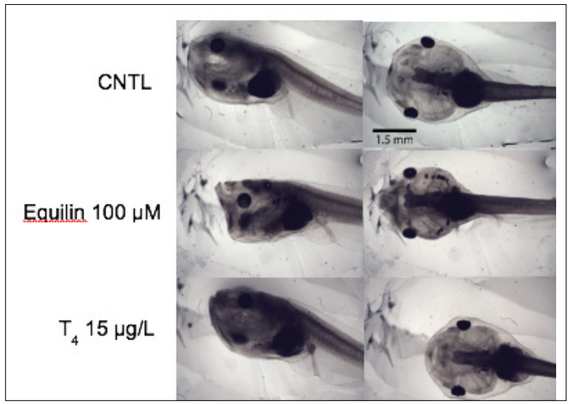

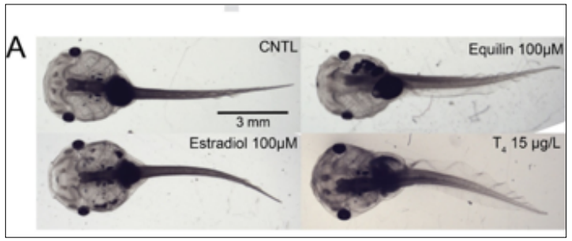

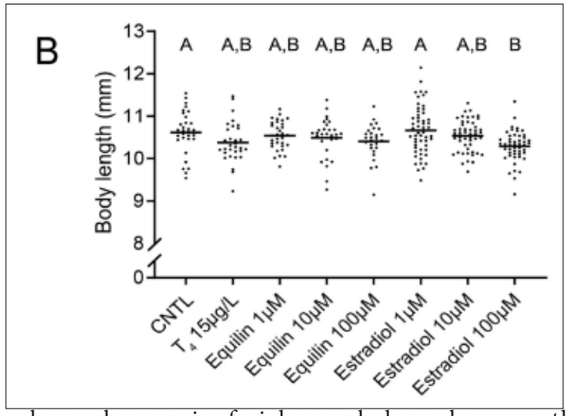

Figure 2) A good indicator of physical development in tadpoles, and their onset through metamorphosis, is body length. A shorter body length typically indicates that they are developing more quickly as they are turning into frogs. Accelerated development is typically seen in thyroid hormone-exposed tadpoles. These images and this Jitterplot show body length for tadpoles sacrificed on Day 4 of exposure. Body length was generally not affected in this experiment, with the exception of estradiol 100 uM. Images were measured using ImageJ imaging software.

Equilin and estradiol increases cell death; T4 does not

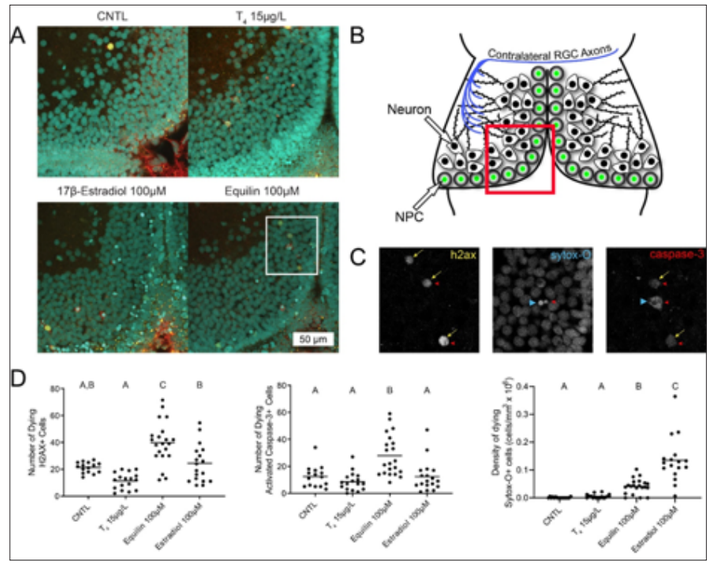

Figure 3) This figure depicts cell death. Figure B is a depiction of cells dividing normally as the brain develops. These dividing cells can also be seen in figure A. Tadpoles were treated with h2ax, caspase-3, and sytox-O; these immuno-stain for cell death. The fluorescing cells in (C) are in the process of dying. **Figure D** shows that thyroid hormone typically reduces cell death if it has an effect at all. However, rather than reducing cell death similarly to thyroid hormone, equilin significantly increased cell death in a manner similar to estradiol.

Cell counting was quantified using ImageJ. Groups with the same letter have similar cell densities. Groups with different letters have cell densities that are statistically different. ($p < 0.05$)

Equilin and estradiol decreases tectum proliferation; T4 increases proliferation

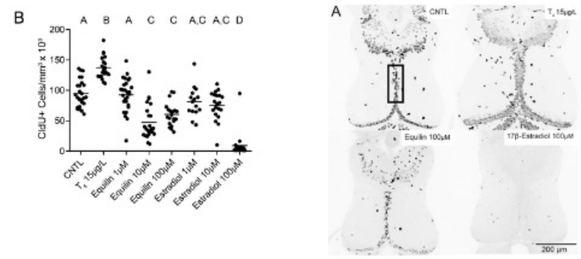

Figure 4) Thyroid hormone exposure typically increases neurogenesis, the division and birth of new neurons. In this experiment, we wanted to see if equilin would also induce increased cell division and neurogenesis. In A, Tadpoles were treated with CldU to immuno-stain for proliferation of neural progenitor cells. Rather than inducing progenitor cell proliferation similarly to thyroid hormone, equilin significantly reduced cell proliferation in

a similar manner to estradiol (B). Cell density was quantified using Imaris imaging software.

Equilin treatment has no effect on expression of TH-sensitive genes in the tadpole brain

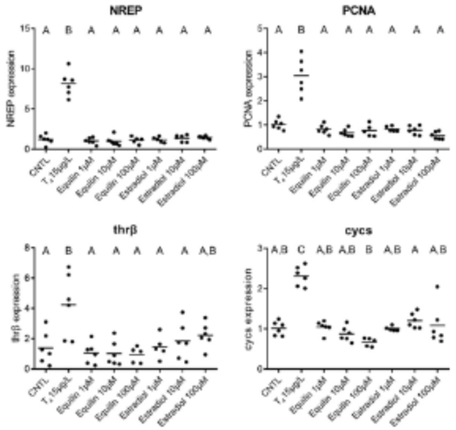

Figure 5) The following experiments used a technique called qPCR to quantify gene expression. We selected a collection of genes that are known to highly express in the presence of thyroid hormone2. We wanted to see if these genes would also express highly in the presence of equilin. qPCR data shows that treatment with 100uM equilin does not increase expression of the following four thyroid hormone sensitive genes: Neuronal Regeneration Related Protein (NREP) (A), proliferation cell nuclear antigen (PCNA)(B), thyroid hormone receptor beta (thrb)(C), or cytochrome c, somatic (cycs)(D). Thus, it is not acting similarly to thyroid hormone.

Conclusions

- Our data do not indicate that equilin induces thyroid hormone- like changes in the developing Xenopus laevis brain. It does not influence expression of thyroid hormone related genes, and it does not induce neural progenitor cell proliferation and changes in brain morphology associated with thyroid hormone signaling.
- Rather, it induces similar morphological changes to 17-β estradiol.
- These data are inconsistent with the assessment of the ToxCast/tox21 dataset and suggests that the Tox21 result is a false positive.

Acknowledgements and References

This work is funded by NIEHS grant R00ES022992 and the Summer Undergraduate Research fellowship in Neuroscience

(1) ToxCast Chemical Landscape: Paving the Road to 21st Century Toxicology | Chemical Research in Toxicology https://pubs.acs.org/doi/10.1021/acs.chemrestox.6b00135 (accessed Jul 8, 2019).

(2) Thompson, C. K.; Cline, H. T. Thyroid Hormone Acts Locally to Increase Neurogenesis, Neuronal Differentiation, and Dendritic Arbor Elaboration in the Tadpole Visual System. J. Neurosci. 2016, 36 (40), 10356–10375. https://doi.org/10.1523/JNEUROSCI.4147-15.2016.

Download poster

Nociceptive detection to electrophilic compounds requires TrpA1, but not painless, in Drosophila

Isiah J. Boyd[1], Victor L. Tran[2], Lina Ni[1]

School of Neuroscience, Virginia Polytechnic Institute and State University

Department of Biological Sciences, Virginia Polytechnic Institute and State University

Abstract

It is essential for an organism's survival to distinguish beneficial food sources from ones that are potentially noxious. Organisms can make these distinctions because of sensory receptors called nociceptors that send signals to the central nervous system in response to potentially damaging stimuli. Subsequently, the organism displays an aversive behavior in response to encountering the noxious chemical. It has been suggested that both *painless* and *TrpA1* are necessary for aversive behaviors to electrophilic compounds in *Drosophila*. We used a modified Two-Choice Capillary Feeding Assay (CAFE) to quantitatively measure aversion to two electrophilic compounds, N-Methylmorpholine (NMM) and Allyl isothiocyanate (AITC), by measuring the exact amount of food consumed. We evaluated the role of *TrpA1* and *painless* by comparing food intake in *Drosophila* with varying genotypes. Wild type control avoided NMM and AITC. The *TrpA1* mutants did not avoid NMM or AITC. However, the *painless* mutants did avoid NMM and AITC. Our results suggest that *TrpA1*, but not *painless*, is required for behavioral aversion to electrophilic compounds, including NMM and AITC in *Drosophila*.

Materials & Methods

Fig. 1a

Figure 1a shows 3-5 day old flies were anesthetized using CO_2 and sorted into ratios of 15 male and 15 female per testing vial.

Fig. 1b

Figure 1b shows 3-5 day old flies were anesthetized using CO_2 and separated by sex.

Fig. 2a

Figure 2a shows flies were starved on a kim wipe that was saturated with deionized water and kept in an incubator at 25°C for a 20-h period.

Fig. 2b

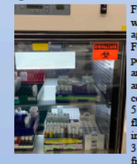

Figure 2b shows flies were starved on 2% agar medium at 25°C. Following a 24-h period flies were anesthetized using CO_2 and sorted into vials containing 5 female or 5 male. Before testing, flies were placed in an incubator at 25°C for 3 hours to recover from the CO_2.

Fig. 3a

Figure 3a shows each testing vial contained four calibrated 5 μL capillary tubes: two containing the control solution and the other two containing experimental solution. The control solution was 3% sucrose. The experimental solution contained 3% sucrose and 5mM AITC or 10mM NMM.

Fig. 3b

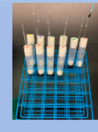

Figure 3b shows each testing vial contained two calibrated 5 μL capillary tubes: one containing the control solution and the other containing experimental solution. The control solution was 5% sucrose. The experimental solution contained 5% sucrose and 5mM AITC. Mineral oil was added to the top of each capillary to prevent evaporation of the solutions.

Fig. 4a

Figure 4a shows after 30 minutes, the amount consumed in each capillary tube was measured in centimeters and a preference index, and mean volume consumed was calculated. Statistical analyses were conducted with GraphPad using a t-Test between sucrose and the experimental containing solutions for each genotype

Fig. 4d

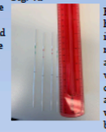

Figure 4d shows after 3 hours, the amount consumed in each capillary tube was measured in centimeters and a preference index, and mean volume consumed was calculated. Statistical analyses were conducted with GraphPad using a t-Test between sucrose and the experimental containing solutions for each genotype.

Results

Fig. 5a

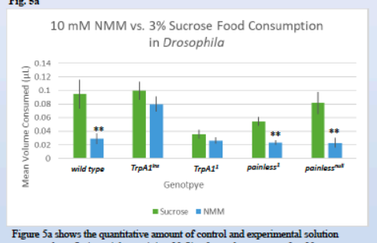

Figure 5a shows the quantitative amount of control and experimental solution consumed per fly in a vial containing 30 flies for each genotype after 30 minutes, following a 20-h starvation period.

Fig. 5b

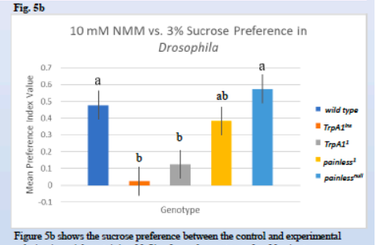

Figure 5b shows the sucrose preference between the control and experimental solution in a vial containing 30 flies for each genotype after 30 minutes, following a 20-h starvation period.

Fig. 6a

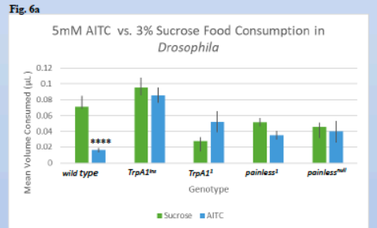

Figure 6a shows the quantitative amount of control and experimental solution consumed per fly in a vial containing 30 flies for each genotype after 30 minutes, following a 20-h starvation period.

Fig. 6b

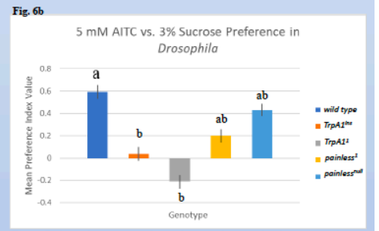

Figure 6b shows the sucrose preference between the control and experimental solution in a vial containing 30 flies for each genotype after 30 minutes, following a 20-h starvation period.

Fig. 7a

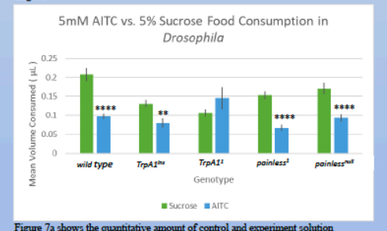

Figure 7a shows the quantitative amount of control and experiment solution consumed per fly in a vial containing 5 flies for each genotype after 3 hours, following a 24-h starvation period.

Fig. 7b

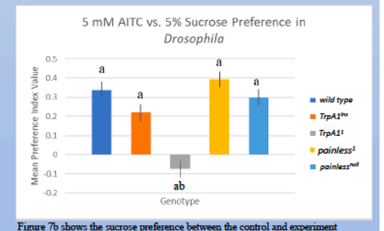

Figure 7b shows the sucrose preference between the control and experiment solution in a vial containing 5 flies for each genotype after 3 hours, following a 24-h starvation period.

Conclusions

- **10mM N-methylmorpholine (NMM) + 3% Sucrose Avoidance:** *wild type*, *painless*^{3} and *painless*^{null} mutants, consumed more sucrose than NMM and preferred sucrose over NMM, where *TrpA1*^{ins} and *TrpA1*$^{\Delta}$ mutants showed no preference for either solution. Therefore, *TrpA1* is required for behavioral aversion to NMM.
- **5mM Allyl isothiocyanate (AITC) + 3% Sucrose Avoidance:** *wild type* consumed more sucrose than AITC and preferred sucrose over AITC. All other mutants showed no preference for either solution nor aversion towards AITC. Therefore, *Trpa1* is required for behavioral aversion to AITC.
- **5mM Allyl isothiocyanate (AITC) + 5% Sucrose Avoidance:** *wild type* and all other mutants, except for *TrpA1*$^{\Delta}$, consumed more sucrose than AITC and preferred sucrose over AITC. *TrpA1*$^{\Delta}$ showed no preference for either solution nor aversion towards AITC. Therefore, *Trpa1* is required for behavioral aversion to AITC.

References

Mandel, Samantha J et al. "Behavioral Aversion to AITC Requires Both Painless and dTRPA1 in Drosophila." Frontiers in neural circuits vol. 12 45. 3 Jul. 2018, doi:10.3389/fncir.2018.00045

Al-Anzi, Bader et al. "Response of Drosophila to Wasabi Is Mediated by painless, the Fly Homolog of Mammalian TRPA1/ANKTM1." Current Biology vol. 16, 10. May 2006: 1034-1040. doi:10.1016/j.cub.2006.04.002

Kang, Kyeongjin et al. "Analysis of Drosophila TRPA1 reveals an ancient origin for human chemical nociception." Nature vol. 464,7288 (2010): 597-600. doi:10.1038/nature08848

Development of Perineuronal nets coincides with astrocytic maturation

Jack L. Browning[1], Cori Whisman[1], Bhanu P. Tewari, PhD[2], and Harald Sontheimer PhD[1,2]

Abstrac:
Perineuronal nets (PNNs) are extracellular matrix assemblies of chondroitin sulfate proteoglycans (CSPGs), tenascin-R, hyaluronan (HA) and link proteins that surround fast spiking parvalbumin (PV) interneurons in the cerebral cortex. PNNs form a lattice like structure around cell soma, axon, and proximal dendrites, and lattice holes are the only available sites for the interacting astrocytes to carry out their housekeeping functions, as well as for axosomatic synapses. In the present study, we explored the developmental timeline of astrocytic maturation and PNN formation to examine whether PNN holes form first- and subsequently define the placement sites for astrocytic endfeet- or, astrocytic maturation and tiling occurs first- defining the sites of PNN holes. To this end, we performed immunohistochemical analysis of PNN structure, excitatory synapses and astrocytic processes using wisteria floribunda agglutinin (WFA), VGlut1 and GFP respectively on Aldh1l1/FVBN/eGFP mice in early postnatal (days 8, 10 and 12), late postnatal (days 20 and 24), and adult (days>60) age groups. We observed astrocytic processes developing over time, concurrently with PNNs in early postnatal groups. In late postnatal groups, PNNs attained their typical lattice like appearance with astrocytic processes and synapses occupying the holes. The immature PNNs were surrounded by astrocytic processes that expressed a surprisingly high level of CSPG, a major constituent of PNNs. Based on the observation of both similar developmental timelines and profound expression of CSPGs in immature astrocytes, we suggest that astrocytes may play an important role in the PNN formation.

Methods:

Animals
All animal procedures were approved and performed in accordance with the ethical guidelines set by Virginia Tech Institutional Animal Care and Use Committee (IACUC). Mice were maintained in groups of five in a specific pathogen-free barrier facility in 12 h light/dark cycles. Male and female ALDH1L1/FVBN/eGFP mice were used at ages P6, P8, P10, P12, P16, P20, P24 and P60 (adult).

Immunohistochemistry (IHC)
Animals of different age groups were injected with a mixture of ketamine and xylazine (100mg/kg and 10 mg/kg respectively). Only P6 mice were anesthetized on ice before and during the procedure. Mice were subsequently trancardialy perfused with phosphate buffered saline (PBS) followed by 4% paraformaldehyde (PFA). The brains were then dissected out and stored overnight in 4% PFA at 4˚C. Next, the brains were transferred to PBS for 48 hrs and 50µm thick floating sections were cut using a vibratome. The sections were then used for IHC or stored at -20˚C in a custom-made cryopreservative medium (10% (v/v) 0.2 mM phosphate buffer, 30% (v/v) glycerol, 30% (v/v) ethylenglycol in deionized water, pH 7.2–7.4) for later uses. The sections used for IHC were then rinsed in PBS and permeabilized and blocked by incubating them in blocking buffer (90% [PBS+ 0.3 % TritonX] + 10% Goat Serum) for 2 hours on a rocking tray. The sections were then incubated with appropriate primary antibodies and biotinylated WFA in diluted blocking buffer (1:3 blocking buffer and PBS respectively) at 4˚C in. On the next day, sections were rinsed in PBS five times for five minutes each and then incubated with appropriate secondary antibodies and Alexa Fluor ® 555-conjugated Streptavidin (1:500 dilution) for 6hrs on a rocking tray in dark. The sections were then rinsed again mounted on glass slides covered with a glass coverslip and sealed with nail polish along the edges of the slide. The primary antibodies used were Chicken GFP (1:500), Rabbit NeuN (1:500) and Guinea Pig VGlut1 (1:1000). The secondary antibodies used were Alexa Fluor Goat anti Chicken 488 (1:500), Alexa Fluor Goat anti Rabbit 647 (1:500) and Alexa Fluor Goat anti Rabbit NeuN (1:500). Images were acquired at different magnifications using Nikon A1 confocal microscope and quantification was performed by inbuilt NIS-Elements AR analysis program as described previously1. High Magnification images in Figures 1a and 1b are snapshots of 3D volume images of 20-30 µm thick z-stacks.

Immunofluorescence intensity quantification
Mean intensity of WFA (CSPGs) was quantified by placing 250 µm x 250 µm ROIs in 10x magnification single plane images. ROIs were placed within L2-3 of the motor cortex, L2-3 of the somatosensory cortex, and within L4-6 of the somatosensory cortex. Within the cortex, CSPGs form bands in the respective layers stated above, starting as clouds of CSPGs and then condensing into PNNs. To reduce variability, these bands were used as the central point for square region placement. Each square region yielded a mean intensity of WFA, which was later averaged from at least three different animals with two different brain sections. The average for each age group was then plotted as graph in Prism and/or origin software.

Line profile intensity
To determine location of astrocytic processes and synapses relative to PNNs, we acquired high magnification (40 x 5) single plane images of individual PNNs and astrocytes in different age groups. A polyline was then drawn along the entire periphery of the PNN expressing cell (Fig.3b). WFA fluorescence intensity of this line shows high intensity peaks and low intensity drops on regular intervals representing areas covered by PNN-CSPGs, astrocytic processes (GFP) and excitatory synapses (VGlut1). We set a threshold of ~50% of highest fluorescence to determine peaks of intensity, and drops in between two peaks of WFA fluorescence that fell below this threshold were considered PNN holes. Peaks of GFP and WFA were denoted by blue arrows, and PNN holes containing astrocytic processes and/or excitatory synapses were denoted by orange arrows (Fig. 3c).

Results:

1. PNNs develop concurrently with astrocytic maturation:
In the present study, PNNs have been seen to begin forming as early as P10 within the somatosensory cortex. This is also the timeline for astrocytic maturation during which they attain their typical bush-like structure and show spatial tiling. Due to the concurrence between PNN development and astrocytic maturation, it is plausible to predict potential physicochemical interactions between the developing PNNs and maturing astrocytes. In our IHC experiments, prior to CSPG condensation into PNNs, we observed clouds of CSPGs within L2-3 and L4-6 of both the motor and somatosensory cortices, beginning at P6 within the somatosensory cortex (SSC) and P10 within the motor cortex (MC) (Fig 1a). Within the SSC at P10, CSPGs begin to condense into PNNs around cell bodies. As CSPGs condense into PNNs and further develop, the mean fluorescent intensity of WFA increases within L2-3 and L4-6 of the somatosensory cortex first at P8 and L2-3 of the motor cortex at P10 (Fig. 1a). Concurrent with PNN development, astrocytic also changed morphologically and exhibited highly ramified and bush-like appearance by P16. In early postnatal development (P6-P12 Fig. 1a) astrocytic coverage area slowly increases, until reaching a stable point in late postnatal development (P16-P24 Fig. 1b). Prior to full astrocytic maturation, especially within P6 and P8, astrocytes appear to express CSPGs, suggesting astrocytes hold the primary role in release of CSPGs into the extracellular matrix. Prior studies have reported that astrocytes release other components to PNNs such as Hyaluronic Acid (HA)2, therefore it is possible that CSPG expressing astrocytes in early development may contribute to the PNN formation by releasing CSPGs.

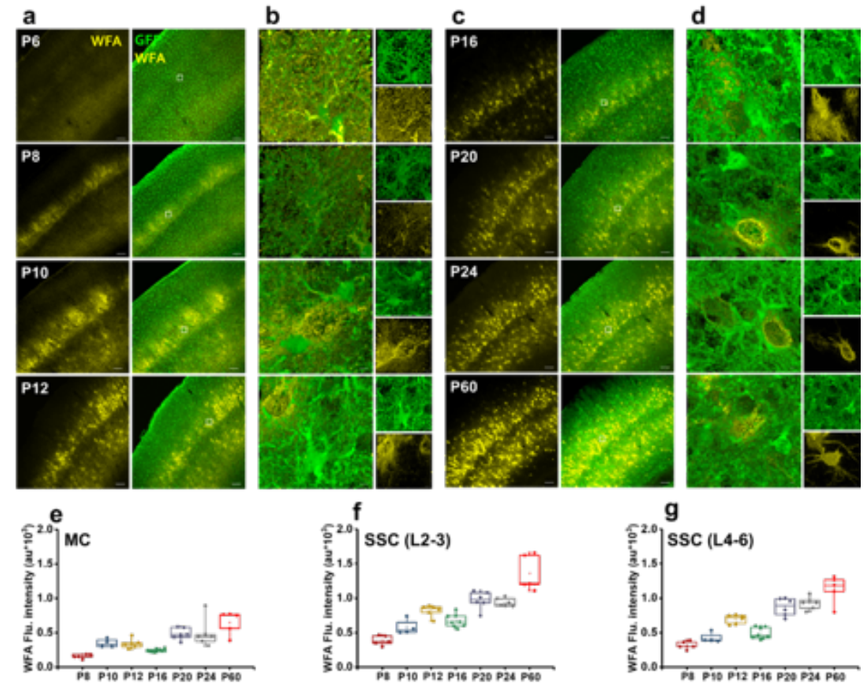

Figure 1: *Expression of PNN-CSPGs and astrocytic maturation during development.*
a. Representative immunofluorescence 10x magnification confocal images of WFA (yellow, left) merged with GFP (Green, right) showing PNN-CSPGs and astrocytes respectively, in somatosensory cortex at early postnatal developmental time points. Scale 100 µm.
b. High magnification (40x5) images (left) of square boxes drawn in a, showing astrocytic maturation (GFP, top) PNN formation (WFA, bottom). Scale 5 µm.
c. Representative immunofluorescence 10x magnification confocal images of WFA (yellow, left) merged with GFP (Green, right) showing PNN-CSPGs and astrocytes respectively, in somatosensory cortex at late postnatal developmental time points. Scale 100 µm.
d. High magnification (40x5) images (left) of square boxes drawn in a, showing astrocytic maturation (GFP, top) PNN formation (WFA, bottom). Scale 5 µm.
e, f, g. Quantified data showing WFA immunofluorescence intensity in L2-L3 of motor cortex (e), L2-3 of Somatosensory cortex (f), and Somatosensory cortex (g). au, arbitrary units of fluorescence.

2. Astrocytes express CSPGs during early postnatal development:
As astrocytes are known to contribute to extracellular matrix formation2, we explored the possibility of astrocytes expressing and releasing the constituents of PNNs including CSPGs, and HA, and thereby contributing to the formation of PNNs. Surprisingly, we observed a remarkable expression of CSPGs along the membrane of astrocytic soma and processes in different cortical layers in early postnatal stages (P6-P10 Fig. 1a). P6 astrocytes in L2-3 of the somatosensory cortex showed highest expression of CSPGs, which gradually decreased by P12 and showed complete absence by P16 (Fig 1a). Astrocytes showing fully mature morphology from adult age group (P60, Fig a) did not show any CSPGs expression. HA expression in maturing astrocytes needs to be investigated yet.

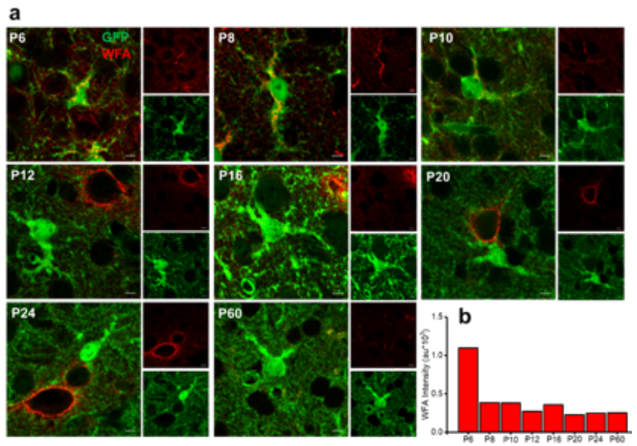

Figure 2: Astrocytes express CSPGs during early postnatal development.
a. Representative high magnification (40x5) immunofluorescence images of WFA (red) merged with GFP (Green) showing PNN-CSPGs and astrocytes respectively, in somatosensory cortex at different postnatal developmental time points. Scale 5 µm. Expression of CSPGs (WFA) can be clearly visualized in P6-P12, which is completely absent in later time points (P20 and P24) and in adult (P60).
b. Representative bar diagram showing mean intensity of WFA in astrocytes at different developmental time points.

3. Spatial proximity of PNN CSPGs, glial processes and synapses in pericellular area
Due to the lattice like structure of mature PNN, the only sites for pre-synaptic terminals and astrocytic processes to interact with PNN-enclosed neurons are within the PNN holes. We studied the pericellular spatial interface between PNN-expressing neurons, excitatory synapses and surrounding astrocytic processes to explore the potential physicochemical interaction during the postnatal development.
We performed high magnification confocal imaging and performed the line profile intensity analysis as explained in the method section. In early postnatal age groups, WFA and GFP immunofluorescence peaks showed remarkable overlap (P6, P8 and P10 Fig. 3c), whereas within late postnatal development and adulthood no such overlap was observed suggesting that astrocytic processes transitioning from an overlapping to non-overlapping spatial interface by primarily occupying the PNN holes (P20, P24 and P60 Fig. 3c). Furthermore, during early postnatal development, astrocytic processes exhibited a closer spatial proximity to PNNs compared to late postnatal development (Fig. 3b). We also observed the presence of excitatory pre-synaptic terminals (using vGlut1), astrocytic processes in the same PNN holes suggesting that PNN holes as sites of tripartite synapses (Fig 3b and 3c). Based on the observance of high CSPG expression and close spatial proximity of astrocytic processes with PNN assembly, we suggest that astrocytes may contribute to the formation of PNN assembly by releasing CSPGs in restricted pericellular sites.

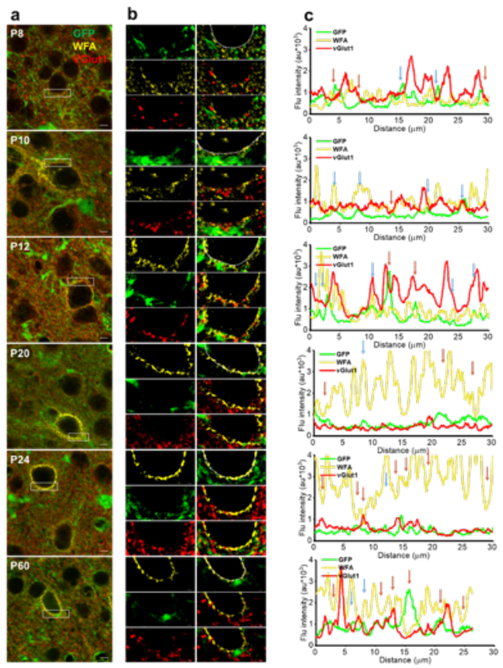

Figure 3: Spatial proximity of PNN, glial processes, and synapses in pericellular area.
a. Representative high magnification (40x5) confocal images showing GFP (green), WFA (yellow), and vGlut1 (red) immunofluorescences in different developmental age groups. Scale 5 µm.
b. Magnified images of rectangular areas (in a), in different combinations of GFP, WFA and vGlut1 fluorescence showing their spatial proximity in pericellular areas. White dotted line represents polyline used to create line profile graphs in c. Scale 1 µm.
c. Line intensity profile graphs of GFP, WFA, and VGlut1 fluorophore intensity over distance of respective age groups. Blue arrows denote overlapping peaks of WFA and GFP, whereas orange arrows denote PNN holes containing astrocytic processes (GFP peaks) and excitatory synapses (vGlut1 peaks). au, arbitrary units of fluorescence.

Conclusion:
Perineuronal nets begin forming during early postnatal development, concurrent with astrocytic maturation. During this period, astrocytes express profound levels of CSPGs and exhibit a close spatial proximity to PNNs and synaptic contacts. During late postnatal development, CSPG expression by astrocytes is not as profound, and close astrocytic spatial proximity to PNNs is primarily limited to PNN holes. Our data suggests that maturing astrocytes may play pivotal role in PNN formation and potentially a PNN mediated physiochemical interaction with PNN-enclosed neurons.

References:
1 Tewari, B. P. et al. Perineuronal nets decrease membrane capacitance of peritumoral fast spiking interneurons in a model of epilepsy. Nature Communications 9, 4724, doi:10.1038/s41467-018-07113-0 (2018).
2 Faissner, A. et al. Contributions of astrocytes to synapse formation and maturation—potential functions of the perisynaptic extracellular matrix. Brain research reviews 63, 26-38 (2010).

Investigating the effects of single cell and network physiology on the performance of spike sorting methods

Reagan Bullins, Lianne Klaver, Kaiser Arndt, Earl Gilbert, Megan Fricke, Payton Hannah, Daniel English
School of Neuroscience, Virginia Polytechnic Institute and State University

Abstract:
Monitoring the activity of neuronal populations at high temporal resolution in behaving animals enables investigation of neuronal interactions supporting behavior. Electrophysiological recording techniques can reveal connectivity and function in neural networks across a range of circuits and systems. Additionally, these techniques are increasingly applied in clinical diagnostic settings (i.e. detection of epileptic loci, brain-machine-interfaces). The current process of extracting spiking data from electrophysiological recordings includes spike detection, feature extraction, and clustering spikes (2). Even the most advanced algorithms for clustering spikes from extracellular recordings currently have low reliability and have not been empirically validated. Errors in spike cluster algorithms may be due to waveform changes along the somatodendritic axis, multiple neurons firing synchronously, single neuron spike train statistics (i.e. bursting), all of which may be unique to different brain regions (1). Our present investigation will determine how these physiological variables contribute to commission and omission errors in clustered datasets by collecting ground truth data in awake mice with a silicon-juxta hybrid probe. This probe allows for extracellular recording of ~ 10-40 neurons, with a coincident juxtacellular recording of one of these neurons. As the juxtacellular technique unambiguously records spikes from single neurons, the combination of these methods constitutes a ground truth for extracellular spike detection. Data are collected from cells in the neocortex, hippocampus, thalamus, anterior cingulate and retrosplenial cortices. This project is working towards identifying the biological variables which interfere with current sorting algorithms, and will enable optimization of these algorithms to minimize cluster sorting errors.

Methods:
Mouse Preparation:
Ground truth data was collected in awake head-fixed C57BL/6J mice with silicon-juxta hybrid probes. The mice were habituated to being head-fixed on a horizontal circular wheel for a span of five training days. Craniotomies were made in the mice over the retrosplenial cortex, hippocampus, and anterior cingulate cortex. These craniotomy locations allowed for access to additional brain regions such as the thalamus and subiculum.
Silicon-Juxta Hybrid Probe Formation:
A silicon-juxta hybrid probe is a juxtacellular glass probe in conjunction with a silicon electrode. Each

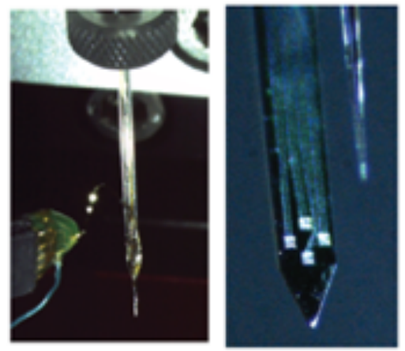

Figure 1. Silicon-juxta hybrid probe formation. *The silicon electrode has 4 recording sites to measure the extracellular space around neurons while the juxtacellular probe measures the intracellular space of a singular neuron. The juxtacellular probe tip was centered above the recording sites of the silicon electrode at an angle of about 10 degrees above horizontal, roughly 25 microns above the silicon electrode's recording sites.*

silicon electrode either had 4 recording sites or 32 recording sites. Juxtacellular probes were formed by putting TW100F-4 glass capillaries (WPI) through a glass puller (Narishige) and filling with 130 mM potassium acetate. The resistance of each juxtacellular probe was checked with a R/C Meter to verify the resistance was between 9-10 MΩ. The juxtacellular glass probe was secured to the electrode with triad gel, a dental adhesive, under a microscope with the aid of micro-manipulators. The silicon-juxta hybrid probes were anchored to robotic micro-manipulators above the head-fixed mice allowing for control of the probe. Currently thirteen successful recordings have been obtained collectively from the lateral parietal association cortex, hippocampus, thalamus, and subiculum.

MATLAB Analysis

The ground truth datasets were spike sorted with the program Kilosort and manually sorted afterwards with the program Klusters. A correlation was found between each extracellular sorted neuron's spike timestamps and the juxtacellular spike timestamps to determine which neuron was being recorded coincidentally by the silicon electrode and juxtacellular probe. The highest correlating neuron was used to determine the accuracy of the spike sorting program Kilosort. The percentage of correct sorted spikes, omission spikes, and commission spikes were quantified.

Results:

The amplitude and frequency of juxtacellular spikes varied across brain regions (Figure 2). The juxtacellular spikes in the thalamus, roughly spanning to 3.5 mV, had the largest amplitudes compared to the hippocampus and lateral parietal association cortex (LPtA) regions. The hippocampus' spikes had the smallest amplitude averaging around 1.2 mV and the LPtA had spikes of about 2.0 mV.

Statistical analysis between the highest correlating extracellular neuron and the juxtacellular datasets revealed the amounts of commission and omission errors. Using Kilosort with identical settings, error rates were different across brain regions (Figure 2). Omission errors include spikes found on the juxtacellular, but not found on the extracellular spike train. Commission errors consist of spikes found on the extracellular spike train, but not on the juxtacellular. The percentage of correctly sorted spikes was lower than the percentages of omission and commission errors.

Discussion & Future Directions:

Intrinsic properties of neurons, such as amplitude and frequency, vary across brain regions. These components may have a role in determining the accuracy of spike sorting programs such as Kilosort.

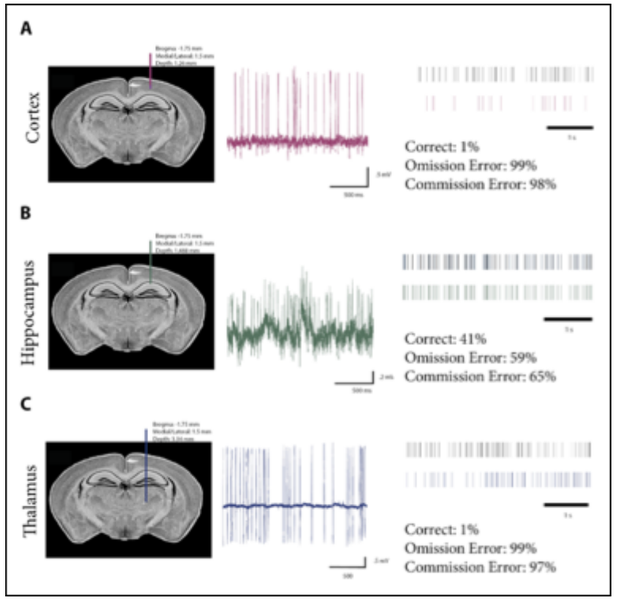

Figure 2. Silicon-juxta hybrid probe recording location, juxtacellular trace, and spike sorting error percentages. *Example silicon-juxta hybrid probe recordings from the lateral parietal association cortex, hippocampus, and thalamus. (A) Left: Recording coordinates for the lateral parietal association cortex is denoted by the colored line representing the silicon-juxta hybrid probe in the given coronal section. Middle: Example raw juxtacellular trace. Right: Raster plot with the top raster line depicting the spikes of the juxtacellular and bottom raster line denoting the spikes of the highest correlating extracellular neuron. The percentages of correct, omission error, and commission error of the sorted spikes is listed.*

(B) Recording summary of the hippocampus.

(C) Recording summary of the thalamus.

The amount of omission errors and commission errors were found to be different for each brain region. Kilosort is spike sorting different neuron populations with the same algorithm which may be leading to the variation in error found in each dataset.

The quantified discrepancies found in the spike sorted datasets could also be a product of other biological variables including waveform change along the somatodendritic axis, cell drifting, cell bursting, and cell synchrony. This project is currently working towards understanding which specific biological variables are causing spike sorting errors and how may spike sorting algorithms be revised to adhere to these issues.

References

1. Harris KD, Henze DA, Csicsvari J, Hirase H, Buzsáki G. Accuracy of tetrode spike separation as determined by simultaneous intracellular and extracellular measurements. Journal of Neurophysiology. 2000 Jul;84(1):401-414.

2. Hazan L, Zugaro M, Buzsáki G. Klusters, Neuroscope, NDManager: A free software suite for neurophysiological data processing and visualization. Journal of Neuroscience Methods. 2006 Sep 15;155(2):207-216.

Monocyte specific EphA4: A Novel Regulator of Tissue Loss in the TBI Milieu

Gabe Coleman[4], Elizabeth A. Kowalski[1], Jiang Chen[1*], Yun Qian[3,5], Michael Chen[1], Xia Wang[1], Amanda Hazy[1], Mingjun Zhou[3,5], Matt Byerly[1], Alicia M. Pickrell[4], John B. Matson[2,5], Irving Coy Allen[1] and Michelle H. Theus[1,4,5]*

1 Department of Biomedical Sciences and Pathobiology, 2 Department of Chemistry, 3 Department of Mechanical Engineering, 4 School of Neuroscience, 5 Center for Regenerative Medicine, Center for Drug Discovery, VA-MD College of Veterinary Medicine, Virginia Tech, Blacksburg, VA

Abstract:

Traumatic Brain Injury (TBI) is a major cause of death and disability and affects 2.5 million people in the United States every year. Following the disruption of the blood brain barrier after TBI, peripheral monocytes infiltrate the injury milieu causing increased inflammation and tissue death. Currently, it is debated whether peripheral monocytes participate in cytotoxicity or wound repair in the TBI environment. It has been previously shown that within hours of initial impact, there is an increase in expression of the tyrosine kinase receptor EphA4 in both humans and mice. Eph receptors are the largest family in the receptor tyrosine kinase class and they carry signals from the cell exterior to the interior by activation from a ligand. EphA4 is responsible for modulating uptake of glutamate, which contributes to synaptic plasticity and increases dendritic spine numbers1. It has been shown that EphA4 global knock out mice are neuroprotective after TBI. In this study, chimeric mice were produced by irradiation and reconstitution with GFP-reporter labeled WT (WTWT-BMC) or EphA4-KO (WTKO-BMC) bone marrow. The WTKO-BMC mice show decreased lesion volume when compared to WTWT-BMC 3 days post-CCI, however when monocytes were depleted these effects were reversed. Implying that EphA4-KO monocytes behave positively in the TBI milieu rather than deleteriously as the WT monocytes do. To investigate the role of monocytes, we performed a depletion and add back with WT or EphA4-KO GFP-reporter labeled monocyte/macrophages. When EphA4-KO monocytes were reintroduced into WT depleted mice (WTKO-PDM), there was a significant decrease in lesion volume when compared to the control and mice given WT monocytes (WTWT-PDM). We further investigated the pro-inflammatory and pro-resolving phenotype of WT and EphA4-KO monocyte/macrophage cultures and found a shift toward pro-resolving phenotype in the EphA4-KO macrophages. This data taken together shows monocyte specific EphA4 promotes a pro-inflammatory phenotype in monocytes/macrophages that exacerbate tissue loss in the TBI milieu and could serve as a therapeutic target to dampen peripheral immune responses following TBI.

Methods

For this experiment, Adult CD1 outbred mice (P60-P90) were used. Before the Controlled Cortical Impact (CCI), which results in a Moderate TBI, the male mice were anesthetized with ketamine/xylazine by i.p. injection. Temperature monitored with rectal probe and maintained at 37˚C. Cortical impact parameters = Craniotomy (right parietal-temporal cortex -2.5 mm A/P and 2.0 mm lateral from bregma): Φ4mm, Depth: 2.0mm, Velocity: 5.0 m/s, Impact duration: 100ms. For our chimeric model, the mice were irradiated to ablate bone marrow. Within 24 hours, mice were given 4x106 BMCs of either WT (control) or EphA4-KO GFP-reporter labeled mice. Mice were given 4 weeks to reconstitute with constant monitoring. Mice were CCI injured 4-6 weeks following bone marrow ablation/reconstitution. Bone marrow cells were harvested from WT and EphA4-KO mice. After extracting the brain, a cryostat was used to make 30 µm serial coronal slices from -1.0 to -2.6 mm posterior from the bregma. 15 slides were used to encompass the entire lesion with 5 slices per slide. To quantify the lesion volume, analysis was performed by estimating the area of tissue loss in the ipsilateral cortical hemisphere for five coronal serial sections around the –1.0 to –2.6 mm posterior from bregma. Nissl stained serial sections were viewed under brightfield illumination at a magnification of 4×. The area of contusion was marked by identifying loss of Nissl staining, tissue death, and tissue hemorrhage. The contoured area, using grid spacing, was then used to estimate total tissue volume based on section thickness, section interval and total number of sections within the Cavalieri program.

Results

Analyzing murine mRNA expression of EphA4 in immune and nervous system cell types, it was shown that humans and mice express comparable amounts post-CCI. Additionally, 2 hours post TBI there is increased EphA4 protein expression in cortices and mRNA expression in peripheral blood. When using immunohistochemistry to stain and analyze EphA4+ GFP+, it was shown that EphA4 is expressed in approximately 68% of infiltrating monocytes 2 days post-TBI. In the Chimeric Model, EphA4 KO bone marrow cells (BMCs) resulted in a smaller lesion volume than the EphA4 WT BMCs. When these mice are depleted after adding either the WT or the KO BMCs, these results are reversed. The depleted EphA4 KO BMCs show a much higher lesion volume than the depleted WT BMCs. Overall, it seems that EphA4 promotes a pro-inflammatory environment, but when EphA4 is knocked out, the TBI milieu becomes more pro-resolving.

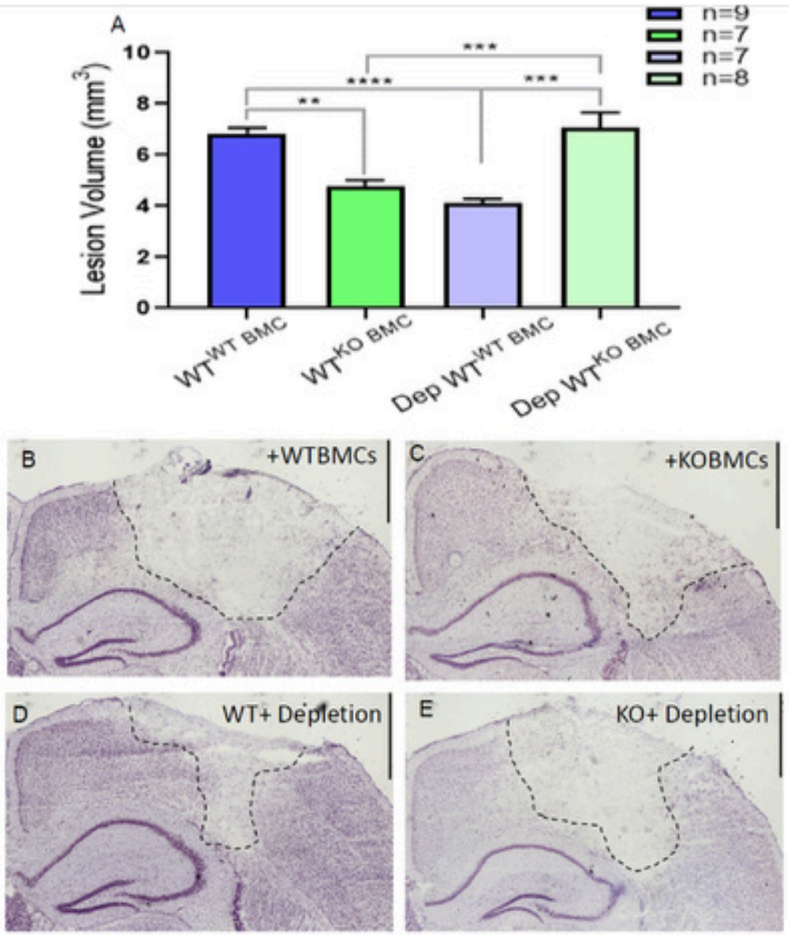

Fig. 4. Depletion of monocyte/macrophages in EphA4 chimeric model. (A) EphA4 KO immune cells display smaller lesion volumes 3d post-CCI injury compared to WT BMCs. WT mice with monocyte depleted also show protection that is attenuated in KO chimeric with depletions. (B) Representative images of $WT^{WT\text{-}BMC}$, (C) $WT^{KO\text{-}BMC}$, (D) $WT^{WT\text{-}BMC}$ + depletion, (E) $WT^{KO\text{-}BMC}$ + depletion.

Conclusions

After a CCI injury, EphA4 is upregulated in whole blood and cortical tissue. When EphA4 KO BMCs are introduced into a mouse, it shows decreased lesion volume when compared to WT BMCs. Alternatively, when monocytes are depleted, the WT-chimeric mice are neuroprotective while the EphA4-KO chimeric mice do not. Overall, we have shown that EphA4 expression on peripheral immune cells contribute to tissue damage after a CCI injury and may contribute to neurotoxicity specifically on monocyte/macrophages.

References

(1) Noberini, R.; Koolpe, M.; Peddibhotla, S.; Dahl, R.; Su, Y.; Cosford, N.D.P.; Roth, G.P.; Pasquale, E.B. J. Biol. Chem. 2008, 283 (43), 29461.

Download poster

Astrocytes as Cellular Players in Maintaining the Blood-Brain Barrier

Deyton Cook[1,2], Ben Heithoff[1], Stefanie Robel1,[2]

Fralin Biomedical Research Institute at Virginia Tech Carillion, Roanoke, VA

VT School of Neuroscience Undergraduate Summer Research Fellowship, Blacksburg, Va

Introduction

The blood-brain barrier (BBB) is a highly specialized interface that restricts entry of bloodborne contents into the brain. When dysfunctional, the BBB allows bloodborne contents into the brain that can cause neuronal cell death and even seizures. While several cell types are known to be involved with the development of the BBB, the cellular contributions to BBB maintenance are not clear. Astrocytes enwrap almost the entire vasculature in their endfeet and secrete factors that can induce BBB properties, but whether they are needed to maintain the BBB in the adult brain is unclear. By ablating some astrocytes, we observed that there is BBB dysfunction suggesting that astrocytes are needed to maintain BBB integrity *in vivo*.

Materials and Methods

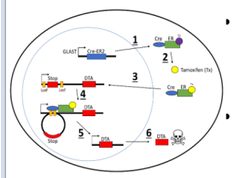

- (1-2) The GLAST promoter, which is only in astrocytes, expresses the CreER unit, an estrogen receptor which tamoxifen (Tx) then binds to the subunit.
- (3-5) This complex then enters the nucleus and allows the transcription of the DTA unit through removing a stop codon.
- (6) DTA is expressed and causes a halt to all protein translation, leading to death.

Tx administered orally

Experimental Genotype: DTA fl/wt, GLAST tg/wt	**Controls Genotype:** DTA fl/wt, GLAST wt/wt or DTA wt/wt,GLAST tg/wt
4 animals given Tamoxifen	8 animals given Tamoxifen

Retro-orbital injection of tracer dye to assess BBB dysfunction in cortex.

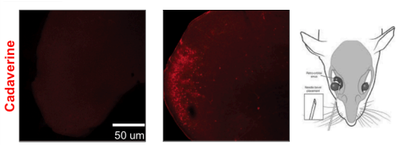

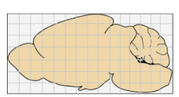

Confocal large area scan taken for 5 slices of each animal.

Quantifying BBB dysfunction

Criteria to quantify leakage:
1) + cell is brighter than background
2) clustered + cells in close proximity
3) Greater than 10 + cells in area

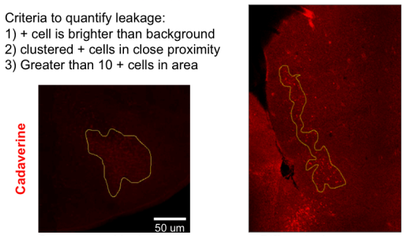

$$5\ slices\ per\ animal \rightarrow \frac{total\ of\ leakage\ areas}{total\ of\ cortex\ area} * 100 = total\ \%$$

Results I

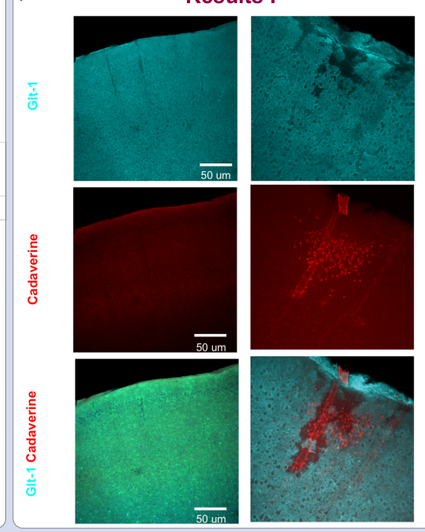

Results II

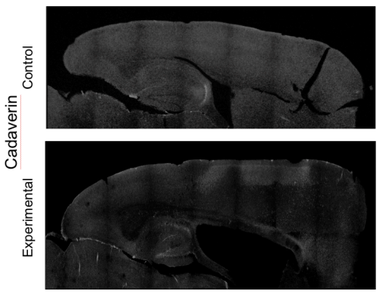

Conclusions

- Astrocyte ablation occurs after tamoxifen administration.
- Ablation of some astrocytes is sufficient to induce BBB dysfunction
- Leakage areas occur in and around Glt1 loss regions
- No other cell types replace astrocytes at barrier to stop leakage.
- Astrocytes are necessary for BBB function because without their presence breakdown occurs.
- Possible errors from quantification were controlled by the researchers being blinded and had guideline to distinguish areas of interest.
- Further steps: What interaction between astrocytes and endothelial cells in the BBB is disrupted when astrocytes are ablated?

References

1. Janzer RC, Raff MC. 1987. Astrocytes induce blood–brain barrier properties in endothelial cells. *Nature*. 325(6101):253–57
2. NIH Office of Animal Care and Use. Rodent Administration Routes. Training Resouces, 6.
3. Yardeni, Tal et al. "Retro-orbital injections in mice." *Lab animal* vol. 40.5 (2011): 155-60. doi:10.1038/laban0511-155

Acknowledgments

I would like to thank everyone a part of the Robel lab for giving me this opportunity. I would like to thank Ben Heithoff for guiding me through this process I could not have done it without him. As well as Dr. Robel for her guidance on this project.

Elucidating the hypothalamic mechanism of glucagon-like peptide 1-induced satiety

Failor Madison, Mark Cline

Neuroendocrinology Laboratory, School of Neuroscience, Virginia Polytechnic Institute and State University

Abstract:
Glucagon-like peptide 1 (GLP-1), consisting of 30-amino acids, is a hormone that also functions as a neurotransmitter which causes a potent reduction in food intake across various species. The precise hypothalamic mechanism mediating this reduction in food intake is unknown in any species, thus our purpose was to elucidate this mechanism. We performed intracerebroventricular (ICV) injections in 7-day-old Japanese quail (Coturnix japonica) with GLP-1 and found a reduction in both food and water intake. A comprehensive behavior analysis revealed that quail injected with GLP-1 had a decreased number of steps, feeding pecks, exploratory pecks, and jumps; while time spent sitting increased. We quantified c-Fos immunoreactivity in key hypothalamic and brainstem nuclei that mediate food intake and determined that the paraventricular nucleus (PVN), ventromedial hypothalamus (VMH), area postrema (AP), and nucleus of the solitary tract (NTS) are active after GLP-1 injection. From this, we plan to isolate the active regions and then use real-time PCR to determine which other neurotransmitters participate in GLP-1-induced satiety. From this a working model of GLP-1 induced reduced food intake should emerge.

Methods:

Animals: Coturnix japonica, Japanese quail (7 days old).

Food and water intake: Birds were fasted 6 hours before the experiment. The quail were randomly assigned to receive an intracerebroventricular (ICV) injection of either a vehicle, a 0.0001, 0.001, or 0.01 nmol dose of GLP-1. Birds were then return to their individual cages and given unlimited access to food and water. Food and water intake were monitored every 30 minutes for 180 minutes post injection.

Behavior analysis: Birds were fasted 6 hours before the experiment. The quail were randomly assigned to receive an intracerebroventricular (ICV) injection of the vehicle or 0.01 nmol of GLP-1, which was determined to be the lowest effective dose in the previous experiment. The birds were then immediately put in clear acrylic arenas with food and water, where they were recorded by 3 cameras for 30 minutes post injection. The data was then collected and analyzed in 5-minute intervals using ANY-MAZE.

c-Fos immunohistochemistry: Birds were fasted 6 hours before the experiment, and were randomly assigned to the treatment or control group. The quail were then intracerebroventricularly (ICV) injected with the vehicle or 0.01 nmol of GLP-1 and returned to their individual cages. Food was removed after injection, to prevent c-Fos immunoreactivity associated with food consumption. 1-hour post injection, brains were sectioned at the hypothalamus and brainstem. An immunohistochemistry assay was performed to identify nuclei with c-Fos expression.

Results:

We first sought to confirm the findings of previous studies, which determined that GLP-1 suppresses food intake. Our food and water intake showed that 0.01 nmol of GLP-1 did indeed decrease food and water intake.

Figure 1. Food intake after injection

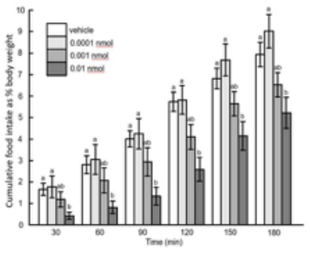

Figure 2. Water intake after injection

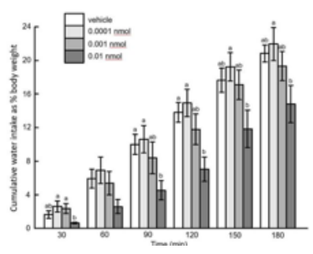

Figures 1 and 2: Cumulative food intake was significantly lower for treatment birds given the high dose, 0.01 nmol of GLP-1 from 30 to 180 minutes, while cumulative water intake was significantly lower for treatment birds given 0.01 nmol at 90 and 120 minutes.

Following the food and water intake, a behavioral analysis was carried out to see if GLP-1 significantly affects any behaviors of the birds.

Behaviors (n)	Treatment	Time post injection (min)					
		5	10	15	20	25	30
Locomotion	Control	1.45±0.44	2.47±0.81	3.53±1.09	4.74±1.45	6.05±1.83	7.62±2.15
	GLP 1	1.08±0.22	1.49±0.26	2.08±0.39	2.67±0.53	3.20±0.59	3.93±0.74
Steps	Control	38.56±9.04	66.96±16.53	97.59±21.74	129.63±28.95	167.67±36.77	211.15±44.86
	GLP 1	25.89±4.06	39.63±5.84	56.89±9.59	74.04±12.22	88.81±14.08	107.96±17.33[b]
Feed Pecks	Control	3.89±1.21	15.22±6.35	36.04±10.34	59.70±15.53	74.19±17.78	98.93±24.21
	GLP 1	0.74±0.46[b]	1.07±0.54[b]	3.07±1.45[b]	6.70±3.84[b]	11.37±7.11[b]	14.96±8.93[b]
Jumps	Control	0	0	0.04±0.04	0.19±0.11	0.26±0.13	0.78±0.33
	GLP 1	0	0	0	0.07±0.05	0.07±0.05	0.07±0.05[b]
Defecations	Control	0	0.04±0.04	0.11±0.06	0.11±0.06	0.15±0.07	0.19±0.08
	GLP 1	0	0	0.04±0.04	0.04±0.04	0.04±0.04	0.07±0.05
Exploratory Pecks	Control	10.07±2.08	18.63±3.64	28.56±4.85	35.85±6.19	45.07±8.55	56.74±10.51
	GLP 1	5.52±1.39[b]	7.70±2.19[b]	10.81±3.57[b]	19.00±7.41[b]	25.48±11.79[b]	29.63±12.70[b]
Escape Attempts	Control	0	0	0	0	0	0
	GLP 1	0.04±0.04	0.11±0.08	0.15±0.12	0.15±0.12	0.15±0.12	0.30±0.21
Drinks	Control	0.44±0.33	0.89±0.50	1.44±0.68	1.93±0.84	2.52±0.90	3.30±0.95
	GLP 1	0.07±0.07	0.19±0.13	0.19±0.13	0.30±0.17	1.11±0.37	1.30±0.41
Perch	Control	1.63±0.72	6.20±1.91	11.29±2.94	20.69±5.47	25.13±6.19	32.18±7.66
	GLP 1	3.40±1.03	14.26±5.90	32.88±16.76	52.22±27.64	62.57±30.09	70.33±30.14
Preens	Control	0.17±0.17	2.11±1.31	5.14±2.49	6.51±2.77	11.99±5.52	15.44±6.80
	GLP 1	0.08±0.08	0.08±0.08	1.39±0.87	1.73±0.98	2.67±1.29	2.78±1.33
Deep Rest	Control	15.23±7.77	36.01±14.13	45.30±18.89	60.93±25.12	75.61±30.21	95.11±33.68
	GLP 1	11.70±6.47	33.84±15.01	52.03±25.22	57.71±25.41	71.25±25.78	87.17±29.88
Stand	Control	273.96±9.54	522.70±20.79	790.37±30.94	1036.61±44.59	1305.27±49.71	1561.19±52.37
	GLP 1	259.75±12.90	473.04±32.08	698.90±47.67	935.45±64.19	1184.20±70.06	1412.37±79.82
Sit	Control	8.79±4.09	35.34±14.57	55.74±25.13	86.23±37.08	94.88±39.48	112.57±41.41
	GLP 1	24.53±9.14	82.22±22.14[b]	124.22±30.41[b]	168.85±42.92[b]	202.56±49.35[b]	249.41±54.71[b]

Table 1: Treatment birds had a significantly decreased number of steps, feeding pecks, exploratory pecks, and jumps. Time spent sitting significantly increased for treatment birds.

A c-Fos immunohistochemistry experiment was then performed to determine what hypothalamic and brainstem nuclei that GLP-1 likely activates.

Figure 3. Difference in c-Fos expression

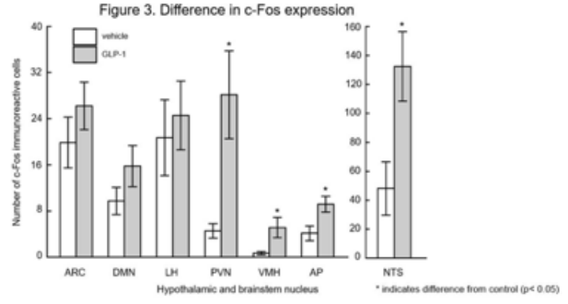

Figure 3: The paraventricular nucleus (PVN), ventromedial hypothalamus (VMH), area postrema (AP), and nucleus of the solitary tract (NTS) had heightened c-Fos expression in treatment birds.

Conclusion

It was determined that GLP-1 suppresses food and water intake in Japanese quail, the effect on food intake is especially potent. GLP-1 injected quail also engaged in less steps, feeding pecks, exploratory pecks, and jumps, but spent more time sitting. The PVN, VMH, AP, and NTS were active after GLP-1 injection. Nucleus-specific gene expression will be examined to further determine the precise mechanism of GLP-1.

References

Baggio LL, Drucker DJ. Glucagon-like peptide-1 receptors in the brain: controlling food intake and body weight. J Clin Invest. 2014;124(10):4223-4226. doi:10.1172/JCI78371

Boyle JG, Livingstone R, Petrie JR. Cardiovascular benefits of GLP-1 agonists in type 2 diabetes: a comparative review. Clin Sci. 2018;132(15):1699-1709. doi:10.1042/CS20171299

Dailey MJ, Moran TH. Glucagon-like peptide 1 and appetite. Trends Endocrinol Metab. 2013;24(2):85-91. doi:10.1016/j.tem.2012.11.008

Donnelly D. The structure and function of the

glucagon-like peptide-1 receptor and its ligands. Br J Pharmacol. 2012;166(1):27-41. doi:10.1111/j.1476-5381.2011.01687.x
Holst JJ. The Physiology of Glucagon-like Peptide 1. Physiol Rev. 2007;87(4):1409-1439. doi:10.1152/physrev.00034.2006
Sandoval D, Sisley SR. Brain GLP-1 and insulin sensitivity. Mol Cell Endocrinol. 2015;418 Pt 1:27-32. doi:10.1016/j.mce.2015.02.017
Shousha S, Nakahara K, Nasu T, Sakamoto T, Murakami N. Effect of glucagon-like peptide-1 and -2 on regulation of food intake, body temperature and locomotor activity in the Japanese quail. Neurosci Lett. 2007;415(2):102-107. doi:10.1016/J.NEULET.2007.01.007

Download poster

Implementing an Early-Life Stress Model that Uses a Limited Bedding Paradigm to Produce Fragmented and Unpredictable Maternal Care

Jessica Maltman, Elizabeth Shupe, Matthew E. Glover, and Sarah M. Clinton
School of Neuroscience, Virginia Polytechnic Institute and State University

Abstract:
Early life stress (ELS) is a known contributor to the development of emotional disorders in humans, such as anxiety and depression. This is primarily due to the fact that early life experiences play a large role in regulating the structural and functional development of brain regions (Walker et al, 2017) and individual neuron function via epigenetic changes (Molet et al, 2014), such as methylation. In rodents, active parental care, which provides sensory input to the brain, is essential for gene expression patterns and the development of stress-related neural circuits (Bolton et al, 2019; Molet et al, 2014). The relation between maternal care and neurodevelopment in rodent pups is explained by the concept of hidden regulators, which rely on different physical stimuli and their patterns to maintain homeostatic balance in systems throughout the body (Walker et al, 2017). Previous rodent studies showed that ELS negatively impacts brain development and later emotional behavior, in part, through disruption of maternal care. For example, one ELS paradigm involves giving rodent mothers (dams) limited bedding and nesting material. The inability to create an adequate nest causes the dams to become stressed and provide fragmented and erratic care. (Walker et al, 2017). The unpredictability of care, occasional maltreatment, and lack of maternal stimuli is believed to induce stress and initiate neuropathology in the rodent pups (Bolton et al, 2019; Walker et al, 2017). Other laboratories have successfully shown that this limited bedding and nesting (LBN) stress model negatively impacts rodent offspring, and the present pilot study aims to establish the LBN stress model in our laboratory in order to study the neurodevelopment of emotional disorders in response to early life stress.
Sprague-Dawley rat litters were randomly assigned to one of three conditions from postnatal day (P)2-P10: a) a control condition with ample bedding; b) a limited bedding and nesting group with 200 mL of bedding and a wire-gauge floor (LBN); and c) a limited bedding and nesting group with 200 mL of bedding and no wire floor (LNW). The frequency and duration of nurturing maternal behavior was observed each morning and evening from P1-P14, and pups' core temperatures and weights were recorded at P2, P10, and P14. At P10, the pups' core temperatures and body weights varied significantly only between the control and LBN group, and at P14, significant differences were found between the bodyweights of the control and LBN group, and the core temperatures of the control and LNW group. Maternal behavior data indicates that the quality and quantity of care provided to the pups is diminished in LB conditions, with less frequent and more sporadic care being an especially stressful situation for the pups. Temperature differences may need to be minimized in the future to prevent cold stress and follow-up offspring behavioral data still need to be obtained and analyzed to determine whether the ELS influenced depression-like behavior.

Methods:

Limited Bedding and Nesting Protocol
Sprague-Dawley rat litters were randomly assigned to one of three environmental conditions from postnatal day (P)2-P10: a) a control condition with ample bedding and 1 paper towel; b) a limited bedding and nesting group with 200 mL of bedding, a ½ sheet of paper towel, and a wire-gauge floor (LBN); and c) a limited bedding and nesting group with 200 mL of bedding, a ½ sheet of paper towel, and no wire floor (LNW). In order to minimize litter effects, any pups born on the same day were randomly assigned to be cross-fostered. This was done by removing all pups from the home cages, sexing the pups using anogenital distance, separating males and females, and returning equal numbers of random male and female pups to the all dams. The pups' core temperatures were measured at (P)2, 10, and 14 using a rectal probe thermometer and petroleum jelly was used to minimize the pups' discomfort. Pups' body weights were also recorded using a standard digital scale at (P)2, 10, and 14. Besides core temperature and bodyweight measurements, cages were left undisturbed until (P)10.
Maternal Behavior Observations
Dams and litters were observed twice daily (once in the light phase and once in the dark phase) from (P)1-P14. Observation sessions consisted of 10 brief ~5 second observations approximately 5 minutes apart for each animal. A checklist of maternal and self directed behaviors, such as whether the dam was inside or outside the nest, nursing, licking or grooming a pup, manipulating nest materials, etc., was used to document maternal behaviors during each snapshot. Precautions were taken while recording behavioral data as to not disturb the dams or pups, such as using red-light headlamps to observe behavior at night.

Results:

Maternal behavior data was used to analyze not only the overall frequency of specific maternal behaviors, such as passive nursing, active nursing, and nurturing behaviors (licking/grooming pups, etc.), but was also used to create a composite behavior score for each housing condition that reflects the fragmentation of maternal behavior. Active nursing, which involves the dam strenuously arching her back to ensure that all pups can nurse, was found to decrease over time regardless of housing condition. Passive nursing, in which the dam is either sleeping or occupied with self-directed behaviors, was found to increase in frequency over time regardless of housing condition. The effect of housing condition on nurturing behaviors was slightly inconclusive, seeing as only some groups had significant interactions during the light cycle, whereas others had significant interactions during the dark cycle, but no overall trends were observed. This implies that overall the frequency of nurturing behaviors may not be significantly affected by housing condition. The amount of fragmentation, determined using a behavior score, trends towards LBN and LNW dams providing more fragmented maternal care during the dark cycle than controls.
The pups' core temperatures and body weights were recorded at several timepoints during the experiment in order to assess overall well-being and potential exposure to cold stress. At (P)2, the LNW group already displayed significantly higher core temperatures than both the control and the LBN groups, implying that there were initial differences. By the end of the experimental period at (P)10, the control pups' core temperatures were significantly higher than the LBN group. After being removed from the housing conditions for several days, at (P)14 male pups in the LNW group had significantly higher core temperatures than the male control pups. For body weight, there were no significant differences between housing conditions at (P)2.
By (P)10, the control pups weighed significantly more than the LBN pups, and this trend remained consistent at (P)14.

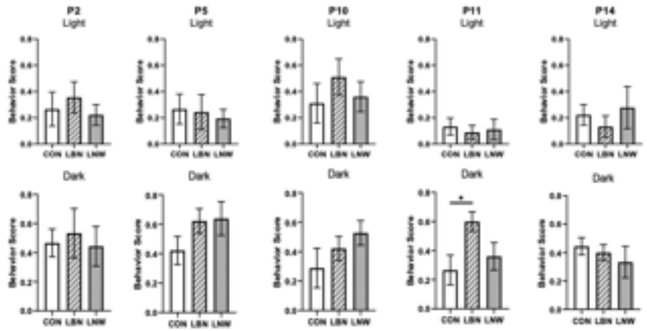

Results Summary: At (P)2, (P)5, (P)10, and (P)14), there were no significant effects of housing condition on behavior score, which is a composite score reflecting how sporadic and fragmented the dam's behavior was during maternal behavior observations. This said, there is a trend towards the dams in the LBN group displaying increased fragmented maternal care than control groups at (P)2, (P)5 during the dark cycle, and (P)10. Additionally, the LNW group displays a trend towards increased fragmentation than controls at (P)5 and (P)10 during the dark cycle. At (P)11 during the day, and (P)14, which is after the dams and litters were removed from their different housing conditions, there are trends towards LBN groups displayed decreased fragmented care than controls. One significant difference between the fragmentation of maternal care was observed between controls and the LBN groups at (P)11 during the dark cycle.

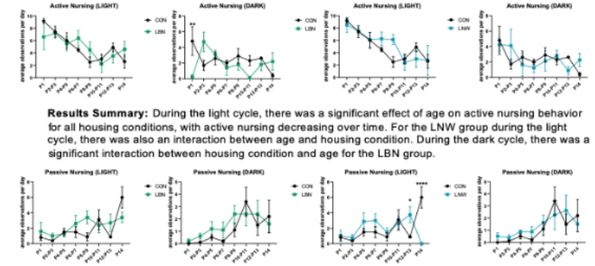

Results Summary: During the light cycle, there was a significant effect of age on active nursing behavior for all housing conditions, with active nursing decreasing over time. For the LNW group during the light cycle, there was also an interaction between age and housing condition. During the dark cycle, there was a significant interaction between housing condition and age for the LBN group.

Results Summary: During the light cycle for all housing conditions there was a significant effect of age on passive nursing behavior, with this behavior increasing with age. Additionally, for the LNW group there was a significant interaction between housing condition and age. During the dark cycle, there was a significant effect of age on passive nursing behavior for all housing conditions.

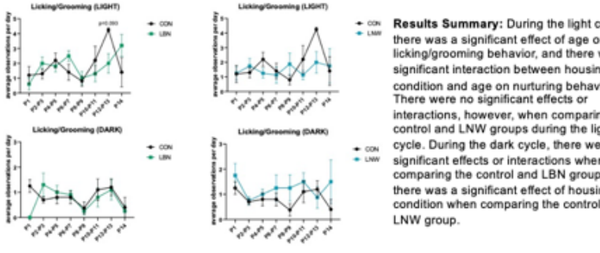

Results Summary: During the light cycle, there was a significant effect of age on licking/grooming behavior, and there was a significant interaction between housing condition and age on nurturing behavior. There were no significant effects or interactions, however, when comparing the control and LNW groups during the light cycle. During the dark cycle, there were no significant effects or interactions when comparing the control and LBN groups, but there was a significant effect of housing condition when comparing the control and LNW group.

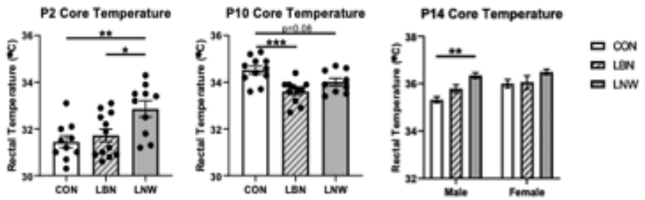

Results Summary: At (P)2, when dams and litters were first exposed to the different housing conditions, the pups' core temperatures were significantly higher in the LNW group than both the control and the LBN group. At (P)10, which was the last day of the different housing conditions, the control groups' temperatures were significantly higher than the LBN group. At P(14), when all groups were in control conditions, male pups in the LNW group displayed higher core temperatures than the control group.

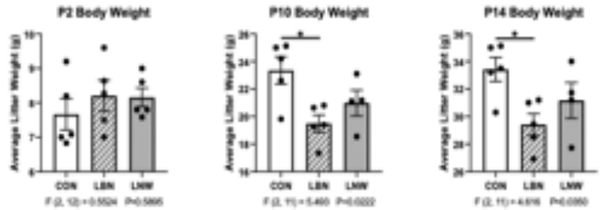

Results Summary: At (P)2, there were no significant differences in body weight when comparing the sexes or housing conditions. At P(10), the pups' body weights in the control group were significantly higher than pups' weights in the LBN group. At P(14), once again, the body weights of the pups in the control group were significantly higher than pups' in the LBN group.

Conclusions (findings and discussion)

Based on the behavioral data describing maternal care, housing condition did not correlate with the quality of maternal care provided, seeing as active nursing, passive nursing, and nurturing behaviors were mainly unaffected by housing condition. These findings are ideal for this ELS due to altered maternal care having confounding effects on pup development and being one of the reasons maternal separation was an inaccurate ELS model. Fragmentation of maternal care, which was represented by a behavior score, however trended towards LBN dams providing more sporadic care than control and LNW dams during the dark cycle. These findings coincide with previous research and are expected to correlate with behavioral data collected in the future.

Offspring body weights were significantly altered after ELS, especially in the LBN condition. This implies that the LBN housing condition itself may adversely affect the wellbeing and development of the pups, or that fragmented maternal care may impede overall pup development. The body weights of the LNW group not being significantly different from the control group suggests that the metal wire itself may be causing the differential effects on body weight.

Seeing as the core temperatures of pups varied significantly at (P)2, before litters were even exposed to the different experimental conditions, it is likely that there were some litter differences in heat regulation, making it difficult to analyze the effect of the different housing conditions on body temperature. This being said, the use of ventilated cages and metal flooring in the LBN group may explain why there is a significant difference in core temperature from the control group at (P)10. Furthermore, at (P)14, the core temperatures appear to follow a similar trend as they did at (P)2, suggesting that after being removed from the housing conditions the pups' core temperatures returned to 'normal'. Cross-fostering more litters in the future may help reduce the initial differences in core temperature.

In order to complete this pilot study, offspring from the different housing conditions will complete a battery of behavioral tests, such as a sucrose preference test, open field test, and forced swim test, in order to characterize depression and anxiety-like behaviors. From the same litters, some offspring will be sacrificed to use their brain tissue to analyze global methylation patterns, gene expression throughout limbic regions, and brain activity in several regions of interest. From there, we will be able to understand critical periods in emotional development, the stress response, and how early life experiences influence behavior.

References

Bolton, J. L., Short, A. K., Simeone, K. A., Daglian, J., & Baram, T. Z. (2019). Programming of Stress-Sensitive Neurons and Circuits by Early-Life Experiences. Frontiers in Behavioral Neuroscience, 13. doi: 10.3389/fnbeh.2019.00030

Molet, J., Maras, P. M., Avishai-Eliner, S., & Baram, T. Z. (2014). Naturalistic rodent models of chronic early-life stress. Developmental Psychobiology, 56(8), 1675–1688. doi: 10.1002/dev.21230

Walker, C.-D., Bath, K. G., Joels, M., Korosi, A., Larauche, M., Lucassen, P. J., … Baram, T. Z. (2017). Chronic early life stress induced by limited bedding and nesting (LBN) material in rodents: critical considerations of methodology, outcomes and translational potential. Stress, 20(5), 421–448. doi: 10.1080/10253890.2017.1343296

Download poster

A stuttering associated mutation in the gene Gnptab alters rat pup ultrasonic vocalizations

Jamie Mustian, Makenzlie Taylor, Tina Taylor, and Mike Bowers

School of Neuroscience, Virginia Tech, Blacksburg, VA

Abstract:

A promising approach to understanding the mechanistic basis of speech is to study disorders that affect speech without compromising other cognitive or motor functions. Stuttering has been linked to mutations in the lysosomal enzyme-targeting pathway, but how this remarkably specific speech deficit arises from mutations in a family of general "cellular housekeeping" genes is unknown. To address this question, we produced a missense mutation in the gene Gnptab. This gene has been associated with human stuttering and has been shown to cause vocal abnormalities in mice. We compared vocalizations from rat pups electroporated with a DNA plasmid engineered to carry a mutation in the Gnptab gene or a scramble control that does not target any known gene in the rat. We found significant differences in the vocalizations of pups with the human Gnptab stuttering mutation compared to controls. Specifically, we found that rat pups with the mutation emitted fewer vocalizations per unit time and had longer pauses between vocalizations and that the tonality of the temporal sequence was significantly reduced. Furthermore, Gnptab mutant rats were similar to control rats on an extensive battery of non-vocal behaviors. These data establish the rat as an attractive model for studying this disorder.

Methods

Ultrasonic Vocalizations:

- Used Ultrasound Microphone (Avisoft UltraSoundGate condenser microphone capsule CM16, Avisoft Bioacoustics, Berlin, Germany) to record the rat vocalizations in a sound attenuating chamber from Metris
- The microphone was placed 30 cm above the rats
- Vocalizations were recorded using Avisoft Recorder software (Version 5.1). Settings included sampling rate at 300 kHz; format 16 bit
- For acoustical analysis, recordings were transferred to DeepSqueak (Version 2.1)
- Spectrograms were generated with an FFT-length of 512 points and a time window overlap of 75% (100% Frame, Hamming window). A lower cut-off frequency of 25 kHz was used to reduce background noise outside the relevant frequency band
- Call detection was provided by an automatic threshold-based algorithm and a hold-time mechanism (hold time: 0.01 s)

Western Blot:

Modified from the methods published in Bowers et al., 2013, in brief:

- All membranes blocked in Licor Buffer (Licor) then incubated in the primary antibody with Licor buffer overnight at 4°C
- One-hour incubation in IRDye-linked secondary antibody
- Detected immunoreactive bands using Odyssey Fc

Behavior

- Social Play, Open Field, and Novel Object

Results

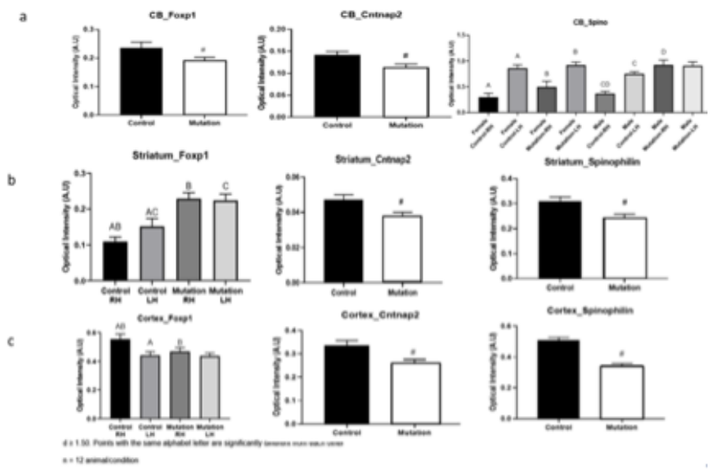

Figure 1: Figures above demonstrate the language associated proteins levels (Foxp1, Cntnap2, and Spinophilin) found in their respective brain region. 1a: The cerebellum demonstrated key differences between the mutant and control for Foxp1 and Cntnap2. Spinophilin in the cerebellum demonstrated sex, condition, and hemispheric variations. 1b: The striatum presented condition differences for Cntnap2 and Spinophilin. Whereas, Foxp1 had hemispheric differences in the control but not in the mutant. 1c: The cortex demonstrated a similar trend to the striatum where significant differences in the two conditions were present for Cntnap2 and Spinophilin.

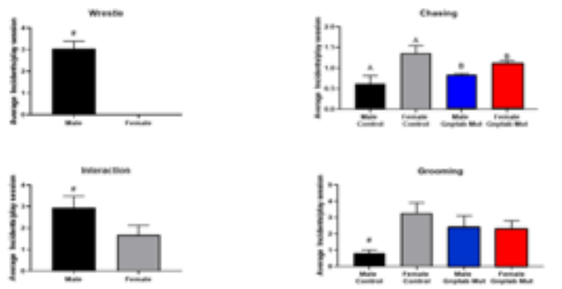

Figure 2: Social play behavior was examined, and four main behaviors were noted as significant. 2a: Wrestling presents a significant sex difference between males and females. Male exhibited more wrestling-like behavior compared to females. 2b: A sex difference was significant for the number of interactions. The total number of interactions was higher in males over females. 2c: Chasing had a sex difference as well as a condition difference. Between the controls, females chased more than males. Between the mutants, females also chased more than males. 2d: Anxious behavior, exhibited by grooming, was more prominent in female controls compared to male controls. No significant difference was found between the mutant males and mutant females.

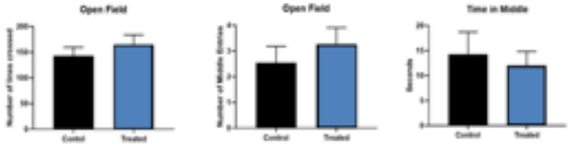

Figure 3: Demonstrates normal behavior in the open field task. No significant differences found between the treated and control.

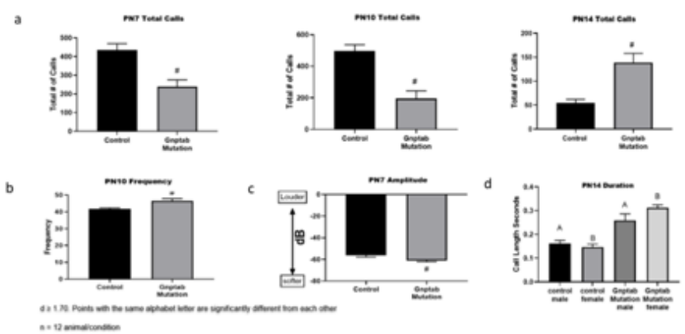

Figure 4: Presents different components of the vocalization data at different postnatal stages. 4a: Postnatal day 7, 10, and 14 all had significant differences between the control and mutant. Total number of calls in the mutant were lower in PN7 and 10, but they were higher in PN14. 4b: PN10 demonstrated a significant difference in the frequency of calls for the mutant. 4c: PN7 controls had louder calls than the mutant. 4d: Sex and condition differences were found in the duration of calls. Both control males and females had a shorter duration than the mutant.

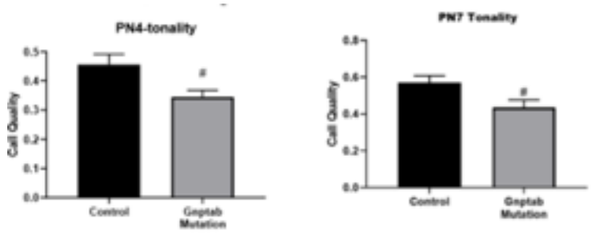

Figure 5: The tonality of the vocalizations at each postnatal stage presented a significant difference between the control and the mutant. The mutant had a lower tonality (quality) of the vocalizations compared to the control at each age.

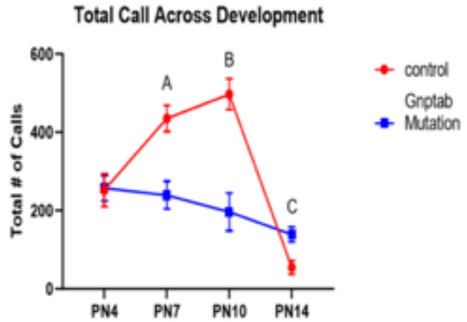

Figurer 6: The total calls for the control demonstrated a normal trend with the calls gradually increasing from PN4 to PN10, then declining from PN10 to PN14. The incline in total number of calls in the younger rats represents cries that would be similar to a human baby cry. The mutant trend is characteristic of stuttering with fewer vocalizations across the stages.

Conclusions (findings and discussion)

Through the Western Blot data, it demonstrated that hemispheric differences in the normal condition are eliminated with the mutation. This is similar to the human condition. Additionally, Foxp1 was concluded to potentially be involved in stuttering. We found significant differences in the vocalizations of pups with the human GNPTAB stuttering mutation compared to controls. Specifically, we found that rats with the mutation emitted fewer vocalizations per unit time and had longer pauses between vocalizations and that the tonality of the temporal sequence was significantly reduced. Furthermore, Gnptab mutant rats were similar to control rats on an extensive battery of non-vocal behaviors. These data establish the rat as an attractive model for studying this disorder

References:

1 Visser, J. C. et al. Variation in the Early Trajectories of Autism Symptoms Is Related to the Development of Language, Cognition, and Behavior Problems. J Am Acad Child Adolesc Psychiatry 56, 659-668, doi:10.1016/j.jaac.2017.05.022 (2017).
2 Simonyan, K. & Horwitz, B. Laryngeal motor cortex and control of speech in humans. Neuroscientist 17, 197-208, doi:10.1177/1073858410386727 (2011).
3 Law, J., Boyle, J., Harris, F., Harkness, A. & Nye, C. Prevalence and natural history of primary speech and language delay: findings from a systematic review of the literature. Int J Lang Commun Disord 35, 165-188 (2000).
4 Yairi, E., Ambrose, N. & Cox, N. Genetics of stuttering: a critical review. J Speech Hear Res 39, 771-784 (1996).
5 Nyby, J., & Whitney, G. Ultrasonic communication of adult myomorph rodents. Neuroscience & Biobehavioral Reviews 2, 1-14 (1978).
6 Sales, G. D., & Pye, D. Ultrasonic communication by animals. (Chapman & Hall., 1974).
7 Whishaw, I. Q., Metz, G. A., Kolb, B. & Pellis, S. M. Accelerated nervous system development contributes to behavioral efficiency in the laboratory mouse: a behavioral review and theoretical proposal. Dev Psychobiol 39, 151-170 (2001).
8 Costantini, F., & D'Amato, F. R. Ultrasonic vocalizations in mice and rats: social contexts and functions. Acta Zoologica Sinica 52, 619-633 (2006).
9 Portfors, C. V. Types and functions of ultrasonic vocalizations in laboratory rats and mice. J Am Assoc Lab Anim Sci 46, 28-34 (2007).
10 Wohr, M., Houx, B., Schwarting, R. K. & Spruijt, B. Effects of experience and context on 50-kHz vocalizations in rats. Physiology & behavior 93, 766-776, doi:10.1016/j.physbeh.2007.11.031 (2008).
11 Wohr, M., Engelhardt, K. A., Seffer, D., Sungur, A. O. & Schwarting, R. K. Acoustic Communication in Rats: Effects of Social Experiences on Ultrasonic Vocalizations as Socio-affective Signals. Curr Top Behav Neurosci 30, 67-89, doi:10.1007/7854_2015_410 (2017).
12 Wohr, M., Seffer, D. & Schwarting, R. K. Studying Socio-Affective Communication in Rats through Playback of Ultrasonic Vocalizations. Curr Protoc Neurosci 75, 8 35 31-38 35 17, doi:10.1002/cpns.7 (2016).
13 Burgdorf, J., Wood, P. L., Kroes, R. A., Moskal, J. R. & Panksepp, J. Neurobiology of 50-kHz ultrasonic vocalizations in rats: electrode mapping, lesion, and pharmacology studies. Behav Brain Res 182, 274-283, doi:10.1016/j.bbr.2007.03.010 (2007).
14 Blumberg, M. S. & Sokoloff, G. Do infant rats cry? Psychol Rev 108, 83-95 (2001).

Download poster

Effect of Variable Stress on T Helper Cell Polarization

Giselle Nicole Rivero Ballon, Jennifer R. Rainville, and Georgia E. Hodes*
School of Neuroscience, Virginia Polytechnic Institute and State University, Blacksburg VA

Abstract:
Globally over 300 million people live with depression, but women are almost twice as likely to be diagnosed. Men and women often have different symptoms of depression, and women tend to have more issues with weight gain or loss, feelings of sadness and melancholy, while men tend to have more difficulty sleeping, feelings of anger and aggressive behaviors. Current treatments for depression fail to adequate relieve symptoms in up to one third of patients, and women are more like to be treatment resistant than men. The mechanism underlying these sex difference are not fully understood, and have not been adequately addressed when developing treatments. Previously we explored the cytokine profiles of men and women with treatment resistant depression, non- treatment resistant depression and healthy controls. Our analysis of cytokine expression in blood samples from patients undergoing depressive episodes suggests the possibility that T helper cell sub populations may be differentially regulated in men and women with depression, and that treatment resistant women experience the strongest dysregulation in cytokines associated with Th1, natural killer T (NKT) cells , and Th17 associated cytokines. Here we present data using a variable stress model to induce T cell changes and explore their relationship to behavioral responses in male and female mice. Female mice are stress susceptible following 6 and 28 days of variable stress, while males are resilient at following 6 days of variable stress, but susceptible following 28 days of variable stress. Our preliminary findings have shown that T helper cells (CD4+) expressed at a higher percentage of the total white blood cell numbers in female mice, but that neither 6 nor 28 days of stress affects the total percentage of CD4+ T cells. We hypothesize that CD4+ T cell differentiation is affected by stress in females, but not males. We will discuss the relationship between individual behaviors from a test battery and numbers of T cell subpopulations, in order to determine the contribution of specific immune cell subpopulations to susceptibility or

resilience to variable stress.

Methods

Animals were C57BL/6J males and females, 8-12 weeks of age from Envigo (Dublin, VA). Mouse procedures were performed in accordance with the Institutional Animal Care and Use Committee guidelines of Virginia Tech. Three stressors were done:
foot shock, 100 shocks over 1 hour/0.45mA/2 sec duration, tail suspension, with tape for 1 hour, and restraint tube, placed in 50mL conical tubes with breathing and tail holes in home cage for 1 hour. Afterwards, a submandibular bleed was done 20 minutes after the final stress exposure. Animals had 24 hours to recover between exposure to the blood draw and the first behavioral test. Flow cytometry was done by drawing directly into FACS buffer, which was transferred into 1 mL of Dextran solution and heated at 37° C heat for 30 minutes to lyse red blood cells. Cells were then given an additional lysis step in red blood cell lysis buffer at room temperature in the dark for 5 minutes. After aspiration of the supernatant Zombie Aqua was added to each sample to identify live vs. dead cells in addition to the following antibody panel: CD8 BV421 (Tc- cell marker), CD183 APC (Th1 cells), CD11b (innate immune cells) , CD194 PE (Th2 cells) , CD4 FITC (T helper cells) , B220 PE-CF594 (B cells). Behavior was then done on all animals. Elevated plus maze was done first. The animal was placed at the end of open and closed arm maze for five minutes in red light. Social interaction followed, where the mice were placed in an open arena for 2.5 minutes with target absent and then for an additional 2.5 minutes with the target present. SI ratio was calculated. Next, splash test was done, where the mouse is sprayed on back with 10% sucrose solution, and is conducted under red light for 5 minutes. Novelty suppressed feeding (NSF) was done with food restriction overnight, latency to eat food pellet in novel area was measured for a 10 minute duration. Lastly, forced swim test (FST) was done. Mice were placed in a 4L beaker with 2.5L water (25+1˚C) for 6 minute duration.
All data was graphed in GraphPad Prism v.8.0.2, using 2-way ANOVA, followed by Tukey's post hoc analysis.

Results:

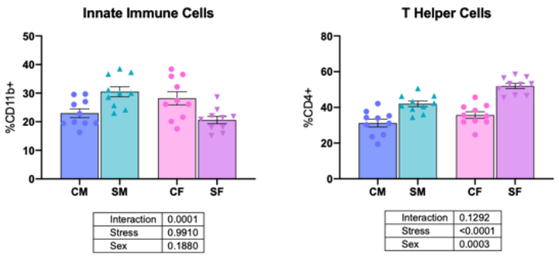

Fig. 1: (A) There was an interaction between sex and stress on innate immune cells. (B) In both males and females stress increased Th cell populations. Females had more Th cells than males. (C) Stress increased the number of cytotoxic T cells (Tc) (D) Stress deceased B cells in both males and females but males had more B cells than females. (E,F) There were no significant effects of stress or sex on Th subtypes.

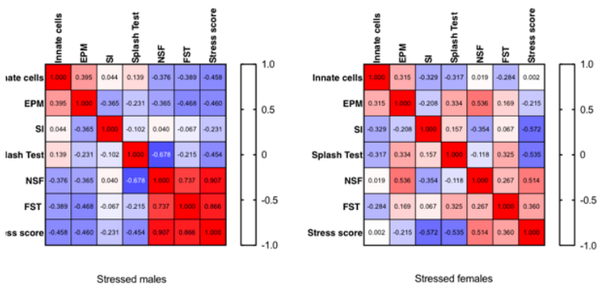

Fig. 2: There is a strong association indicated between stress score vs. NSF (r=0.907), and stress score vs. FST (r=0.866) in males after 6 day variable stress. There is also a strong association between FST and NSF (r=0.737). There is a moderate association between innate cells and the stress score in stress males (r=-0.458). There were no significant associations between any of the variables for stressed females.

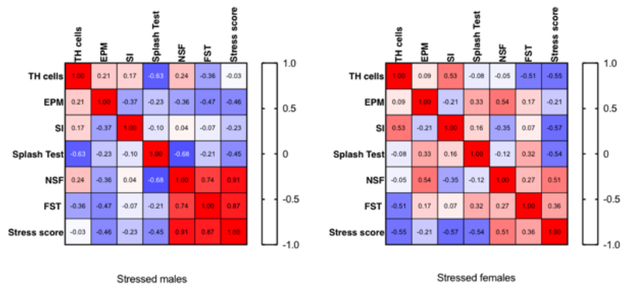

Fig. 3: There is a strong association indicated between stress score vs. FST (r=0.87) and NSF (r=0.91) in males after 6 day variable stress. There is also a strong association between FST and NSF (r=0.74). There were no significant associations between any of the variables for stressed females. There is a moderate association between TH cells and stress score in stress females (r=-0.55).

Conclusion:

We see opposite effects of variable stress on innate immune cells in males and females. The increase in innate immune cells in males may be related to their behavioral resilience. Both males and females have increased Th and Tc cells following stress. In females there may be a relationship between Th cell population and stress susceptibility scores. Both males and females have decreased B cell populations following 6 days of variable stress. Sex differences in behavioral stress susceptibility and resilience may be more related to innate immune responses in males and adaptive immune responses in females. In the future, we will examine additional subtypes of innate and adaptive cells. We will also manipulate cell populations to determine their role in behavioral stress susceptibility. We also will isolate and sequence immune cells in males and females to examine the cell type specific molecular signatures of stress susceptibility in the peripheral immune system.

References:

1. Hamad, ARA. et al. Hybrid lipids, peptides, and lymphocytes: new era in type 1 diabetes research. J Clin Invest. 130. (2019).
2. Gomez-Olarte, S. et al. Intermediate Monocytes and Cytokine Production Associated With Severe Forms of Chagas Disease. Front Immunol. 10. (2019).
3. Rothermundt, M. et al. Inflammatory Markers in major depression and melancholia. J. of Affective Disorders. 63, 93-102 (2001).
4. Maes, M. et al. Leukocytes, Monocytes, and Neutrophilia. J. of Psychiatry. 26, 125-134 (1992).
5. Ambreé, O. et al. Social Defeat Modulates T Helper Cell Percentages in Stress Susceptible and Resilient Mice. Int J Mol Sci. 20. (2019).

Download poster

Altered Metabolic Activity and Hippocampal Changes in Stress Reactive Rats Exposed to Maternal Separation

Sedovy MW, McCoy CR, Kamboj S, Jackson NL, Kerman IA, Clinton SM
School of Neuroscience. Virginia Polytechnic Institute and State University

Abstract:
Early life stress (ELS) is widely accepted to have a range of effects on brain development and behavior, although it is most often associated with negative effects such as increased anxiety, depression, and stress susceptibility in adulthood. Evidence from our laboratory suggests that ELS can lead to adaptive behavioral changes and increased stress resiliency in certain individuals. We found that exposing rats that naturally display high stress reactivity and anxiety/depression like behavior, the Wistar Kyoto (WKY) rat, to ELS (daily 180-min maternal separation from postnatal days 1-14) lead to improved adult depression- and anxiety-like behavior. ELS-exposed WKY male offspring also showed increased hippocampal DNA methylation, suggesting an epigenetic mechanism for the adaptive behavioral effects. The current study built upon our earlier findings by studying male and female WKY offspring to determine whether similar changes occur in both sexes. We first found that ELS lead to increased DNA methylation in the hippocampus of male WKY rats, but not females. To assess other ways that ELS changes the WKY hippocampus, we are investigating markers of cellular metabolism in the hippocampus, focusing on activity of cytochrome C oxidase (COX), the rate limiting enzyme in the production of ATP. Our results so far indicate that ELS leads to diminished COX activity in the dentate gyrus of WKY males compared to controls, with no apparent effects in females, and no significant changes in the cornu Ammonis (CA) region of the hippocampus. Additional analyses are examining COX activity in other brain regions that regulate emotional behavior, such as the amygdala and prefrontal cortex. Overall, the results of this study will help to understand the adaptive neuronal changes that contribute to increased stress resilience in ELS-exposed WKY rats, which may ultimately point to novel biological mechanisms to pursue for treatment of stress-related disorders such as depression.

Methods:

WKY male and female rat pups were randomly assigned at P0 to either the MS or NH group. The MS group was separated from their dam for 180 minutes daily and the NH was separated for 15 minutes daily. This occurred between 8:30am and 12:00pm from P1

to P14. Separated pups were transferred to a separate cage and placed on an approximately 37°C heating pad for the duration of the separation. After P14, pups were undisturbed until P21 when they were weened. Animals of the same group and sex were housed three to a cage and underwent weighing and standard cage changes weekly. Behavioral testing was performed once the animals reached P60.

MS Alters DNA Methylation in Adult WKY Hippocampus

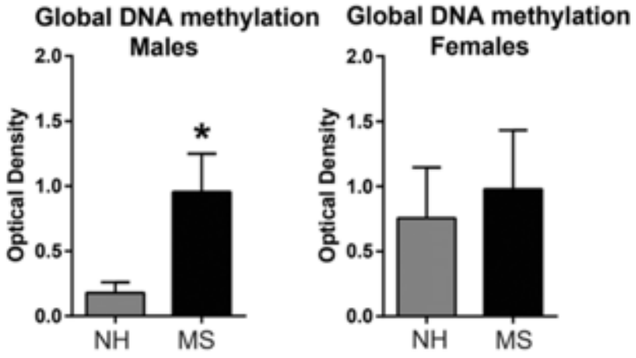

DNA methylation levels were measured in adult WKY male and female rats who were exposed to either maternal separation (MS) or neonatal handling (NH) in early life. MS exposed males showed a significant increase in hippocampal DNA methylation levels (p-value (t-test) *=P<0.05).

Behavior

A. Novelty Suppressed Feeding (NSF)

B. Forced Swim Test (FST)

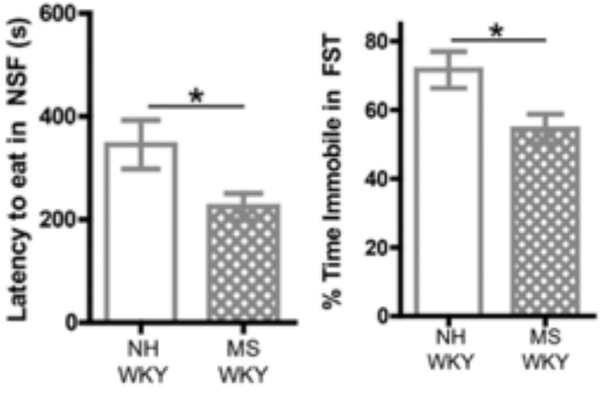

Experimental group WKY pups were subjected to 180 minutes of maternal separation (MS) daily on postnatal days 1-14. Control animals were subjected to neonatal handling (NH) for postnatal days 1-14. Adult male offspring (n=12-15/group) were put through a battery of behavioral tests. MS animals

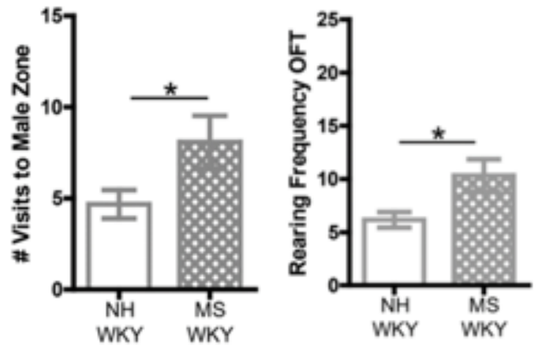

C. Social Interaction

D. Rearing Behavior in the Open Field Test (OFT)

displayed decreased anxiety-like behavior in the Novelty Suppressed Feeding Test (A). FST immobility was also decreased in the MS group (B). MS animals showed more social investigation behaviors in the Social Interaction Test (C). In the Open Field Test, animals in the MS group displayed more rearing behavior then the NH group, indicating a decrease in anxiety-like behavior (D); corrected p-value (t-test)*=p<0.05

Cytochrome C Oxidase (COX)

Amygdala

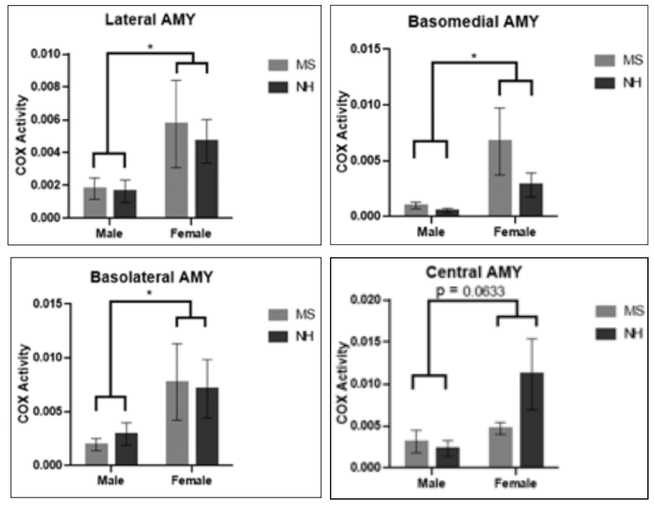

Cytochrome C Oxidase (COX) activity was analyzed using Image J image analysis software. The lateral, basolateral, and basomedial amygdala all displayed significant differences between males and females (p-value (2-way ANOVA) *=P<0.05) and the central amygdala showed a trend in the same direction (p=0.0633). No significant effect of ELS was observed.

Prefrontal Cortex

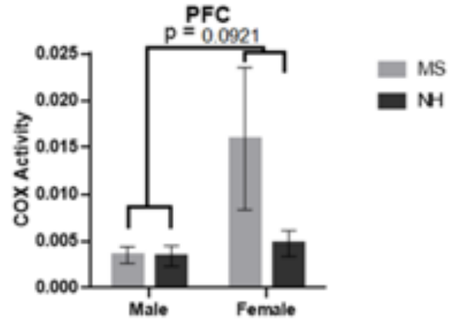

Cytochrome C Oxidase (COX) activity was analyzed using Image J image analysis software and a trending difference was found between males and females (p-value (2-way ANOVA).

Results, Conclusions, and Future Directions

Maternal separation significantly altered behavior in the WKY rats. MS animals displayed less depression- and anxiety-like behavior as well as an increase in social behavior. Hippocampal DNA methylation was also elevated in MS males. Hippocampal volume was not significantly altered. This suggests a possible epigenetic mechanism for the changes in behavior. COX activity saw significant or trending differences between the sexes in both the amygdala and the prefrontal cortex. This significance warrants further exploration into the effects of MS on COX activity, specifically in females. Future directions include more work with female WKY rats including methylation or acetylation levels in the amygdala and running behavioral tests. Investigation into COX activity in the HPC is also in progress.

References

(1) McCoy, C. R.; Rana, S.; Stringfellow, S. A.; Day, J. J.; Wyss, J. M.; Clinton, S. M.; Kerman, I. A. Eur. J. Neurosci. 2016, 44 (10), 2829–2845.
(2) Rana, S.; Pugh, P. C.; Jackson, N.; Clinton, S.M.; Kerman, I. A. Neurosci. Lett. 2015, 584, 146–150.

Download poster

Reconstituted Mining Effluent Reduces Neuronal Proliferation in the Developing Brain and Slows Growth of Body Features in Wild-Caught Wood Frog Tadpoles

Hannah G. Sturgeon, Jeremy P. Kitchen, Lara I. Dahora, Sara E. Sweeten, Christopher K. Thompson

Abstract:
Mining has been a dominant industry in rural Appalachia for more than 150 years, but the impact of mining on aquatic animal health is not well understood. This is an important issue because Appalachia is home to an enormous diversity of organisms, including a huge array of amphibians that live in streams that receive mining effluent from operating and abandoned mines. We examined the effects of reconstituted mining effluent on the development of wood frog (Lithobates sylvaticus) tadpoles. We collected day-old fertilized eggs from a creek near Blacksburg, VA in early March 2018 and raised them to hatch. Tadpoles were then assigned to either sulfate or chloride-based reconstituted mining effluent treatment groups diluted to six different conductivities (100 µS/cm - 2,400 µS/cm). After 7 or 14 days of treatment, tadpoles were euthanized and fixed in paraformaldehyde. In the initial experiment, brains were immunostained for phospho-histone3, which labels dividing progenitor cells in the brain. These experiments suggested that mining effluent that has high concentrations of sulfate is particularly likely to negatively impact the brain development of amphibians. These results piqued our interest in the potential effects of reconstituted mining effluent on cell death in the developing amphibian brain. In the follow-up experiment, we chose to use a subsection of the treatment groups, this time only using the lowest (100 µS/cm) and the highest (2400 µS/cm) conductances. To investigate the effects of reconstituted mining effluent on cell death, we immunostained for Caspase-3 and H2A.X, which label dying cells in the brain. This experiment did not yield the results we expected, as the images instead showed labeling in groups of puncta within the neuropil region of the tectum. At this point the identity of these puncta is unknown, but we plan to perform future experiments to uncover what is being labeled.

Methods:

Animals: Lithobates sylvaticus tadpoles (7 &14 days old).

Tadpole Collection: Potential spawn sites were checked daily for eggs. On the first day eggs were found, they were collected so the exact age would be known. Harvested eggs were allowed to hatch in lab.

Treatment: At 7 days post-fertilization, tadpoles were transferred to treatment groups of either sulfate or chloride-based reconstituted mining effluent diluted to six different conductivities (100 µS/cm - 2,400 µS/cm).

Groups of tadpoles were reared in the solution for either seven or fourteen days.

High sulfate simulated mining effluent

	Calcium sulfate	Magnesium sulfate	Sodium bicarbonate	Potassium chloride	Sodium chloride
grams per 100 L H2O	86	68	32	2	2

High chloride simulated mining effluent

	Calcium chloride	Magnesium chloride	Sodium bicarbonate	Potassium chloride	Sodium chloride
grams per 100 L H2O	86	68	32	2	2

Sacrifice and tissue processing: Tadpoles were euthanized on Day 7 and Day 14 post-treatment with an overdose of MS222 and fixed overnight in 4%PFA. Standard immunohistochemistry methods were used to stain whole-mount brains for

- Initial project: pH3 (Sigma, 1:1000) and Sytox-O (Life Sciences, 1:500)
- Follow-up project: Caspase-3 (abcam,1:500) and H2A.X (EMD Millipore,1:500)

Imaging and analysis: Prior to dissection, animal's heads and bodies were imaged on a Nikon Model C-DSS115 microscope for later morphological analysis. PFA-fixed brains were imaged on a Leica DM6 CFS confocal microscope, and images were analyzed using both ImageJ and Imaris.

Chloride-based reconstituted mining effluent decreases proliferation only at Day 14

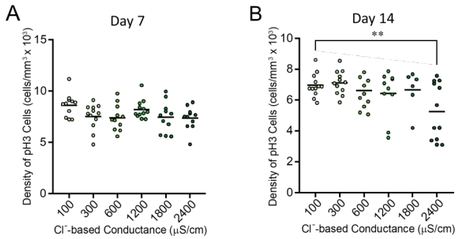

Scatter dot plots showing density of phosphorylated Histone-3 (pH3)+ cells in the ventricular zone for tadpoles sacrificed on A) Day 7 and B) Day 14. Chloride-based reconstituted mining effluent showed no significant differences at Day 7 and significantly lowered progenitor cell division at 2400 µS/cm at Day 14 relative to control. ** = p< 0.01

Reconstituted mining effluent slows growth of morphological features

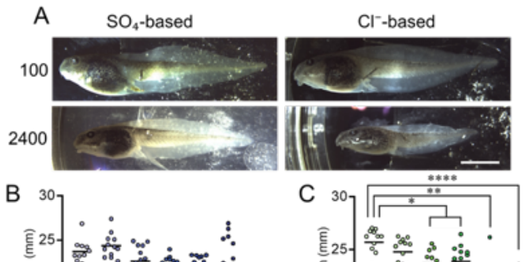

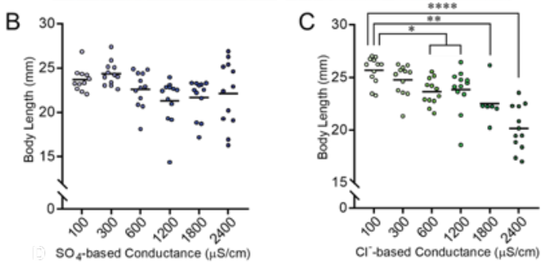

A) Images of example Day 14 tadpoles at 100 µS/cm and at 2400 µS/cm exhibiting body length. Scale bars represent 5 mm. B) Scatter plot showing the effects of sulfate-based mining effluent on body length at Day 14. C) Scatter plot showing the effects of chloride-based mining effluent on body length at Day 14. Chloride-based reconstituted mining effluent significantly slowed the growth of morphological features at Day 14. Sulfate-based effluent has less of an effect and showed an increase in variability at higher concentrations. * = p<0.05, ** = p< 0.01, **** = p< 0.0001

Sulfate-based reconstituted mining effluent decreases proliferation in the optic tectum

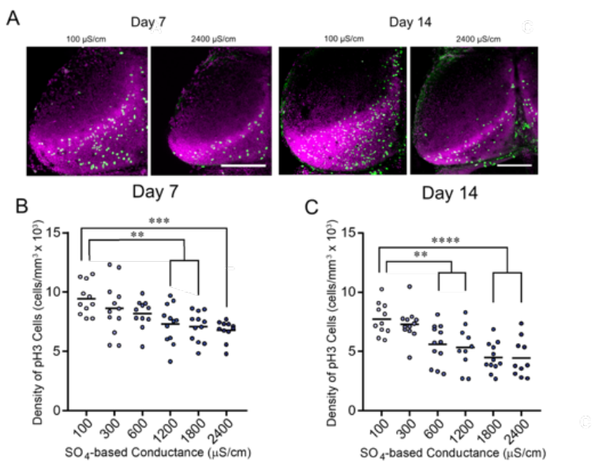

A) Z-projections of confocal stacks of the left hemisphere of the optic tectum from exemplar tadpoles treated with 100 µS/cm and 2400 µS/cm from Day seven and Day 14. Scale bars represent 200 µm. Scatter dot plots showing density of phosphorylated Histone-3 (pH3)+ cells in the ventricular zone for tadpoles sacrificed on B) Day 7 and C) Day 14. Sulfate-based reconstituted mining effluent significantly lowered progenitor cell division at 1200 µS/cm at Day 7 and at 600 µS/cm at Day 14 relative to control. ** = p< 0.01, *** = p< 0.001, **** = p< 0.0001

Limited evidence of cell death in the optic tectum of wood frog tadpoles

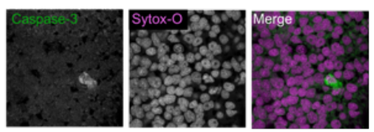

Images of a dying cell in the 600 µS/cm sulfate-based mining effluent group. Showing the Caspase-3 stain, the Sytox stain, and the merged channels. We found very few Caspase-3 positive cells in the brain which made quantification moot.

Density of unidentified puncta in the neuropil region of the optic tectum was lower in 2400 µS/cm SO_4-based mining effluent

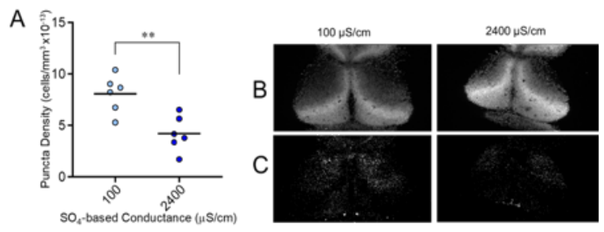

A) Scatter dot plot showing density of puncta in the neuropil region of the optic tectum. Z-projections showing the B) Sytox stain and the C) H2A.X labeled puncta regions.

Conclusions:

- Sulfate-based reconstituted mining effluent significantly lowered progenitor cell division at 1200 µS/cm at Day 7 and at 600 µS/cm at Day 14 relative to control.
- Chloride-based reconstituted mining effluent was less impactful, with no significant differences observed at Day 7 and significantly lowered progenitor cell division at 2400 µS/cm at Day 14.
- Chloride-based reconstituted mining effluent slowed growth of body length.
- Higher concentrations of mining effluent appeared to increase variability of morphological features within each treatment.
- These experiments suggest that mining effluent that has high concentrations of sulfate is particularly likely to negatively impact the brain development of amphibians.

Citations:

This work is funded by NIEHS grant R00ES022992, the Global Change Center Undergraduate Research Grant, and the Summer Undergraduate Research Fellowship in the School of Neuroscience.

Download poster

Assessing Brain Microvasculature in a Model of Von Hippel-Lindau Mutations and the Potential Application of Ultrastructural Analysis

Rachael E. Ward, Sarah Taylor, Vanessa Bradley, Karen Paralkar , John Chappell

Virginia Tech School of Neuroscience, Blacksburg, VA, Fralin Biomedical Research Institute

HYPOTHESIS

The presence of genotypic changes previously demonstrated in the VHL model used in the Chappell lab have been correlated to several physiological changes in several tissues around the body. Since these changes are consistently found in other regions of tissue this should carry over to the brain in the form of changes in vascular density, physiology and morphology.

ABSTRACT

Von Hippel-Lindau (VHL) syndrome is a genetic condition involving the growth of tumors (e.g. clear cell Renal Cell Carcinoma) and hyper-vascularized lesions in various tissues throughout the body including the retina, cerebellum, and brain stem. This condition is characterized by distinct vascular changes like increased vessel branching and aberrant vessel remodeling via several pathways such as the Notch pathway. Hemangioblastomas, a type of vascular tumor, develop in the cerebellum and brain stem in the human condition. The goal of this project is to identify the development of these tumors and other morphological changes within the cerebellum microvasculature in a *Vhl* loss and Type 2B mutation mouse model. The Chappell Lab has previously characterized a mouse model for these *Vhl* mutations in which gene expression and vessel morphology in the retina aligned closely with the human condition (Arreola et al. 2018). To extend this previous study, the current project involved imaging the vasculature within the cerebellums of several mice induced to experience genetic variations of *Vhl* and compare the vascular networks to littermate control mice. To accomplish this, vibratome-cut sections of postnatal day 21 (P21) and P22 mouse cerebellum were immunostained for vascular cells. These sections were imaged by confocal microscopy with a specific interest in expected changes in vessel branching and the potential presence of vessel-derived tumors. In addition, we sought to develop a protocol for observing ultrastructural changes in the vessel walls of *Vhl* mutant cerebellums. We utilized data sets from the Fox Lab (Fralin Biomedical Research Institute) acquired by Serial Block Face-Scanning Electron Microscopy (SBF-SEM) to examine physiological features of the microvasculature in the brain of wild-type mice. Applying SBF-SEM to analysis of *Vhl* mutant brain vasculature could be helpful in defining the precise spatial relationships between endothelial cells, pericytes, and smooth muscle cells in the brain microvasculature.

INTRODUCTION

- Our lab is interested in **pericytes**
  - A mural cell found in the basement membrane of vascular
    - These cells play a role in vascular stability
    - We are specifically interested in how the relationship between pericytes and endothelial cell changes in vascular effecting diseases like **VHL**
- VHL is a genetic based disorder caused by mutations that effect the regulation of HIFs and VEGF
  - These mutation effect notch signaling and vessel physiology
  - In the human condition hemangioblastomas develop in the Cerebellum and in the kidneys clear cell Renal Cell Carcinoma (ccRCC)
    - These are vascular tumors
  - We study the 2b mutation which effect vessel branching and maturation

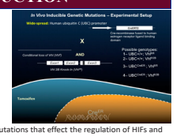

METHODS

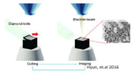

Serial Block Face- SEM

- Ultrastructural cell detail
  - Can see organelles, membranes and cell location
  - Cannot be stained
    - Cells identified by shape and location

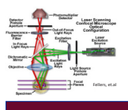

Confocal Microscopy

- High resolution images of tissue in 2D and 3D space
  - Utilizes immunohistochemistry to identify cell types and extracellular matrix proteins

RESULTS: CONFOCAL IMAGING

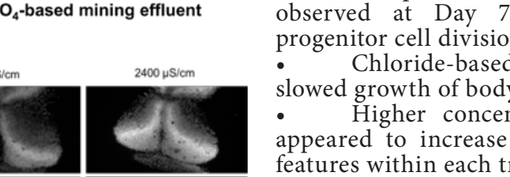

- Figure 1 shows the successful stain of a pericyte (NG2) in the cerebellum of a wild-type mouse
- Figures 2 shows the same NG2 stain from Figure 1 with less success
- Figure 3 shows an interesting feature of the vasculature found in the cerebellum
- Figure 4 demonstrates where in the cerebellum the images came from

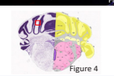

RESULTS: SERIAL BLOCK FACE SEM

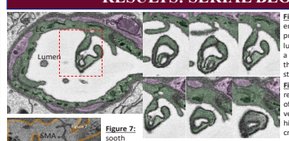

Figure 5: endothelial projection into lumen creating a semi-circular then circular structure

Figure 6: 3D reconstruction of a blood vessel in the hippocampus- created in FIJI

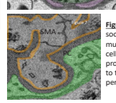

Figure 7: sooth muscle cell projects to the pericyte

Figure 8: Pericyte projection towards the lumen without cell membrane compromise

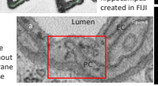

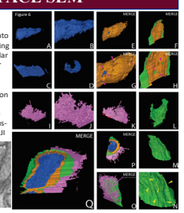

- Intentional structural changes exposed through this method of imaging
  - There are multiple occurrences of most of these structural interactions
- Study the physiology of the basement membrane
  - How it changes in thickness to allow the vasculature to preform different functions in the brain

Figure 9/10: Figure 9 shows an endothelial cell protruding from the side of the blood vessel. Figure 10 looks like an endothelial cell but has an uncharacteristic protrusion.

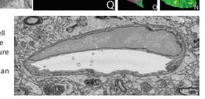

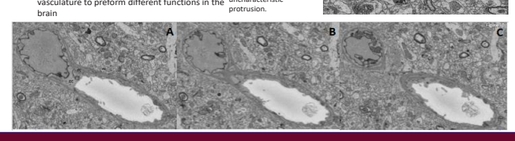

RESULTS: SBF-SEM ECM THICKNESS

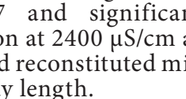

Figure 11: a This figure shows changes in ECM thickness particular to one vessel believed to contain a vSMC

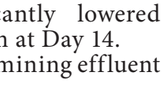

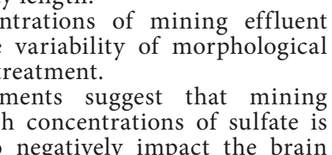

Figure 12: a graph showing changes in ECM thickness measured from SBF-SEM data with an n of 8

CONCLUSIONS

- Despite the issues we have had staining for pericytes, especially those in the brain, it is possible and can help answer questions about changes in pericyte density and blood vessel physiology
- SBF-SEM shows a lot of promise as a concrete method of filing in the gaps left by confocal microscopy
  - Gives basement membrane detail that can't be created with the resolution on confocal microscopy.
  - This technology could help our lab answer questions about diseases that effect basement membrane thickness and orientation

FUTURE DIRECTION

- Full brain scans with confocal microscopy
  - This will help address changes in vessel branching, density
- Expanding SBF-SEM to the VHL model to examine differences in vascular physiology and basement membrane composition
- Expand the use of imaging to Super Resolution microscopy to quantify changes in vascular composition in both VHL and WT models

REFERENCES

Beazley-Long N, Durrant AM, Swift MN and Donaldson LF. The physiological functions of central nervous system pericytes and a potential role in pain [version 1; referees: 2 approved]. *F1000Research* 2018, 7(F1000 Faculty Rev):341 (doi: 10.12688/f1000research.13548.1)

Hyun Kim, Gyu & Won Gim, Ja & LEE, KEA JOO. (2016). Nano-Resolution Connectomics Using Large-Volume Electron Microscopy. Applied Microscopy. 46. 171-175. 10.9729/AM.2016.46.4.171.

Arreola, A., Payne, L. B., Julian, M. H., Cubas, A. A. D., Daniels, A. B., Taylor, S., Zhao, H., Darden, J., Bautch, V. L., Rathmell, W. K., and Chappell, J. C. (2018) Von Hippel-Lindau mutations disrupt vascular patterning and maturation via Notch. *JCI Insight*3.

Acknowledgements
- Fox Lab- SBF-SEM Data
- Rathmell Lab- VHL Mouse Line

CONTACT: wrachael@vt.edu

Neonatal overexpression of a truncated variant for Foxp1 alters ultrasonic vocalizations in rats

Lauren Weaver, Nicole DeFoor, Makenzlie Taylor, Tina Taylor, Mike Bowers

School of Neuroscience, Virginia Tech

Abstract:
FOXP1 is a member of the Forkhead Box (FOX) gene family of transcription factors, which includes four members, FOXP1/2/3/4. Fundamental to shaping brain development, FOXP1 is highly implicated in understanding neurodevelopmental disorders and has a well-known connection to both language and autism. Exome sequencing of humans with intellectual deficits and autism has revealed several truncated FOXP1 mutation variants. These mutation variants have been hypothesized to produce a dominant-negative effect on transcriptional activity. A common phenotype of individuals with FOXP1 mutation variants includes profound deficits in speech and cognition. We discovered a naturally occurring truncated variant of FOXP1 which shares many characteristics with the mutation variants found in humans. To test whether this naturally occurring variant impacted vocalizations, we electroporated rat pups with a DNA plasmid engineered to carry either this truncated variant or a scramble control that does not target any known gene in the rat. We found significant differences in vocalizations: the truncated FOXP1 pups emitted a reduced total number of vocalizations and produced vocalizations at higher frequencies compared to the vocalizations of control pups. We also found altered protein levels for downstream targets of FOXP1. These data suggest the natural variant of FOXP1 has biological relevance for the shaping of the neural circuits responsible for vocalization in rats.

Methods

Ultrasonic Vocalizations

- Avisoft Bioacoustics UltraSoundGate condenser microphone was used to record rat vocalizations in a Metris sound attenuating chamber via Avisoft Recorder software (V 5.1).
- For analysis, recordings were transferred to DeepSqueak (V 2.1)
- Spectrograms were generated with an FFT-length of 512 points, a time window overlap of 75%, and a cut-off frequency of 25 kHz
- Call detection was provided by an automatic threshold-based algorithm and a hold-time mechanism (hold time: 0.01 s)

Behavior

- Social play, novel object, open field

Western Blot

- Modified from Bowers et al., 2013, in brief:
- All membranes blocked in Licor Buffer (Licor) then incubated in the primary antibody with Licor buffer overnight at 4°C
- One-hour incubation in IRDye-linked secondary antibody
- Detected immunoreactive bands using Odyssey Fc

Immunocytochemistry

- Same as Bowers et al., 2014

Results:

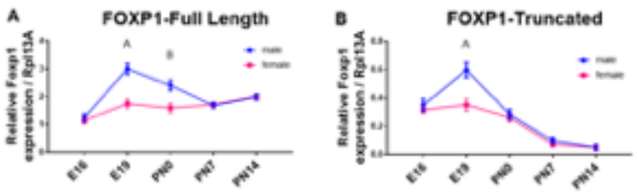

d ≥ 1.10. Points with the same alphabet letter are significantly different from each other
n = 8 males and 8 females each time point

PCR data revealed sex differences between the expression of the full-length Foxp1 variant (Foxp1-FL) and the truncated variant (Foxp1-TR). Interestingly, an androgen burst occurs only in male rats at embryonic day 19.

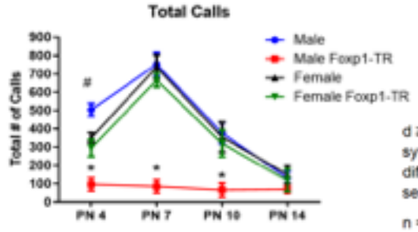

d ≥ 1.20. Points with the same symbol are significantly different from each other. # = sex difference

n = 12 animals/condition

The number of ultrasonic vocalizations (USVs) was significantly reduced in the control male rats compared to all other groups.

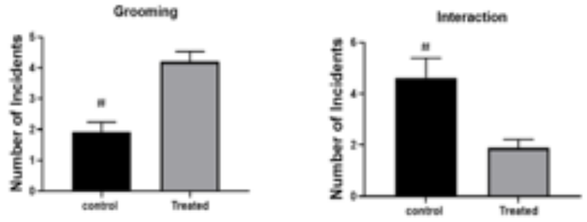

Social play behavioral data for both male and female treated rats demonstrated an increase in anxiety behaviors such as grooming and a decrease in social interaction.

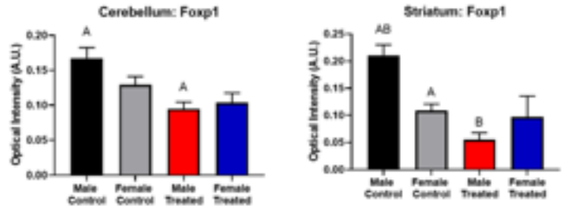

d ≥ 1.43. Points with the same alphabet letter are significantly different from each other

n = 12 animals/condition

Western blot data for regions of the brain responsible for language such as the cerebellum and striatum demonstrated the significant differences in the amount of Foxp1-FL expressed between all experimental groups, with the treated males exhibiting the lowest levels of Foxp1-FL.

Conclusions

Foxp1-TR has biological relevance for the shaping of the neural circuits responsible for USVs in rats. The male treated rats produced significantly fewer USVs than all other rats at various ages throughout development, indicative of a potential sex difference which corresponds with an androgen burst in utero observed only in male rats. Foxp1-TR is also associated with a reduction in socialization and an increase in anxiety behaviors in rats, similar to the autistic phenotype in humans. As such, Foxp1 may influence the male predisposition to autism via androgen receptors on the gene. Future research may investigate further sex differences between social play behaviors, as well as search for transitional patterns across juvenile vocalizations, test for protein-protein interaction, and investigate possible androgen receptor binding interaction.

References

1. Frohlich, H., Rafiullah, R., Schmitt, N., Abele, S. & Rappold, G. A. Foxp1 expression is essential for sex-specific murine neonatal ultrasonic vocalization. Hum Mol Genet 26, 1511-1521, doi:10.1093/hmg/ddx055 (2017).
2. Teufel, A., Wong, E. A., Mukhopadhyay, M., Malik, N. & Westphal, H. FoxP4, a novel forkhead transcription factor. Biochim Biophys Acta 1627, 147-152, doi:10.1016/s0167-4781(03)00074-5 (2003).
3. Tang, B. et al. Forkhead box protein p1 is a transcriptional repressor of immune signaling in the CNS: implications for transcriptional dysregulation in Huntington disease. Hum Mol Genet 21, 3097-3111, doi:10.1093/hmg/dds132 (2012).
4. Bowers, J. M. & Konopka, G. The role of the FOXP family of transcription factors in ASD. Dis Markers 33, 251-260, doi:10.3233/DMA-2012-0919 (2012).
5. Sollis, E. et al. Identification and functional characterization of de novo FOXP1 variants provides novel insights into the etiology of neurodevelopmental disorder. Hum Mol Genet 25, 546-557, doi:10.1093/hmg/ddv495 (2016).
6. Sollis, E. et al. Equivalent missense variant in the FOXP2 and FOXP1 transcription factors causes distinct neurodevelopmental disorders. Hum Mutat 38, 1542-1554, doi:10.1002/humu.23303 (2017).
7. Carr, C. W. et al. Chiari I malformation, delayed gross motor skills, severe speech delay, and epileptiform discharges in a child with FOXP1 haploinsufficiency. Eur J Hum Genet 18, 1216-1220, doi:10.1038/ejhg.2010.96 (2010).

Download poster

DOCC Function in Cool Avoidance in Drosophila Melanogaster Larvae

Jin Yoon, Jackson Wilbourne, Jordan Tyrrell, and Lina Ni*

School of Neuroscience, Virginia Tech, USA

Abstract:
Being able to differentiate between favorable and dangerous environments is critical for animals. We use Drosophila melanogaster to understand how animals find their optimal temperatures. Previous studies identified that the Dorsal Organ Cool Cells (DOCCs) and their molecular cool receptor, composed by three members of the Ionotropic Receptor family, IR21a, IR25a and IR93a, are required for avoiding cool temperatures in 1st and early 2nd instar larvae. In this study, we focused on 72 hour after egg laying (AEL) larvae, also known as early 3rd instar, and 120 hour AEL larvae, late 3rd instar. Our previous data

showed a change in D. melanogaster's temperature preference from 24°C, preferred by early 3rd instar, to 18°C, preferred by late 3rd instar. Here, we found that a functional block of DOCCs drove larvae to a cooler temperature at early 3rd instar, but not late 3rd instar. It is also seen that the activation of DOCCs drove avoidance in both early and late 3rd instar larvae. Taken together, these results suggest that DOCCs are necessary for cool avoidance at early 3rd instar, but not late 3rd instar. Surprisingly, DOCCs are sufficient for the avoidance behavior in both early and late 3rd instar larvae.

Introduction

Drosophila Melanogaster have an optimal temperature that they prefer. In order to adjust to its preferred temperatures, their behavior shifts accordingly. As D. Melanogaster develops through its stages, their preferred temperatures shifts. During their early third instar larvae, around 72 hours after egg laying (AEL), they have a preference for 24°C. However, during their late third instar larvae, or around 120 hours, their preferred temperature changes to 18°C.

In order to understand the underlying mechanism of this switch in temperature preference, this project focused on IR21a. The other identified IRs which are in the Dorsal Organ Cool Cells, such as IR93a and IR25a, have different functions such as olfactory, thermosensory , and hygrosensory abilities. Unlike these IRs, IR21a is specific to cool perception. Because of this, we wanted to test the sufficiency and necessity of this IR in DOCCs.

Therefore, to test the significance of this ionotropic receptor, we used a temperature gradient and optogenetics to observe larvae behavior when cells stopped expressing IR21a.

Materials and Methods

Temperature Gradient Assay

A temperature gradient was established in order to observe which temperature the larvae preferred. The gradient was set from 13°C to 31 °C and were placed in the middle of the gradient and were timed for 15 minutes. Pictures of the gradient were taken each at 10:00, 12:30, and 15:00 minutes. Data were averaged from 9 trials of each fly line.

Optogenetics

A larva was placed in the middle of the petri dish and was allowed to rest for 30 seconds. The larva was then exposed to light 10 times, each for 5 seconds, once every 15 seconds. Number of turns were recorded and averaged after 30 trials.

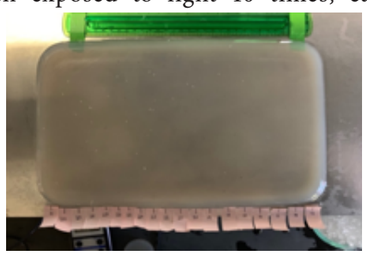

Figure 4. Temperature gradient

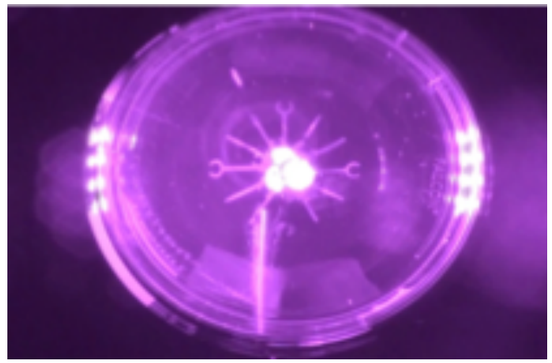

Figure 5. Optogenetics plate

Results

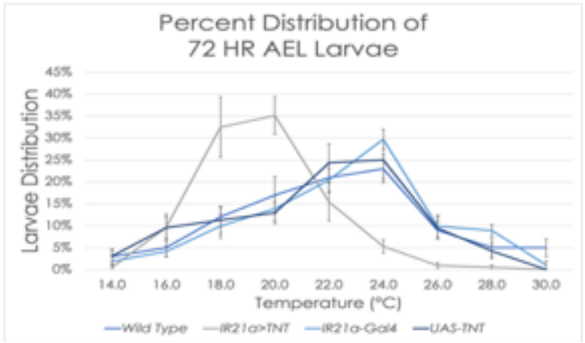

Figure 2a. Shows the temperature preferences of 72 hr AEL larvae

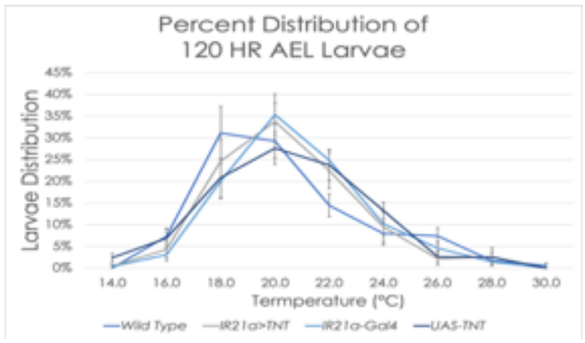

Figure 2b. Shows the temperature preferences of 72 hr AEL larvae

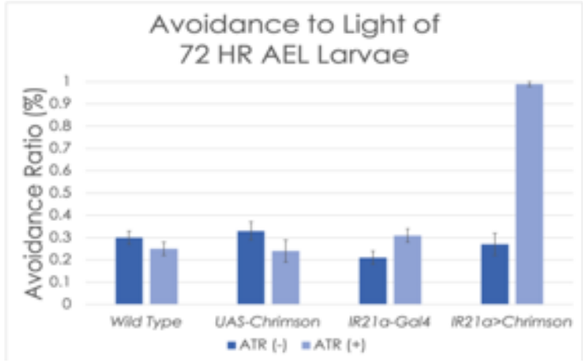

Figure 3a. Shows the percent of avoidance to light of 72 hr AEL larvae

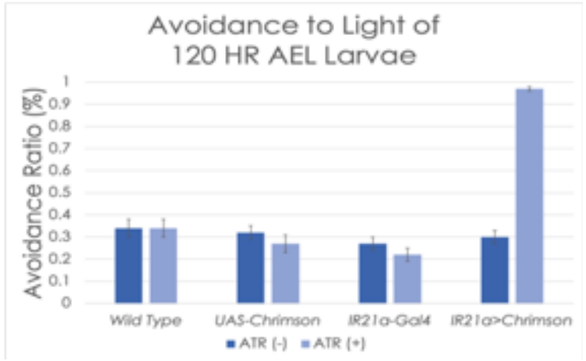

Figure 3b. Shows the percent of avoidance to light of 120 hr AEL larvae

Conclusions

From our data, we were able to conclude that when the function of DOCCs was blocked, the larvae preferred a cooler temperature at early 3rd instar but not late 3rd instar which shows that IR21a is necessary for cool avoidance at early 3rd instar

Furthermore, the activation of DOCCs drove avoidance in both early and late 3rd instar which shows that it is sufficient for avoidance before in both instars.

References

1. Klein, M., Afonso, B., Vonner, A. J., Hernandez-Nunez, L., Berck, M., Tabone, C. J., … Samuel, A. D. T. (2015). Sensory determinants of behavioral dynamics in Drosophila thermotaxis. Proceedings of the National Academy of Sciences, 112(2), E220–E229. https://doi.org/10.1073/PNAS.1416212112

2. Ni, L., Klein, M., Svec, K. V, Budelli, G., Chang, E. C., Ferrer, A. J., … Garrity, P. A. (2016). The Ionotropic Receptors IR21a and IR25a mediate cool sensing in Drosophila. ELife, 5. https://doi.org/10.7554/eLife.13254

3. Knecht, Z. A., Silbering, A. F., Ni, L., Klein, M., Budelli, G., Bell, R., … Garrity, P. A. (2016). Distinct combinations of variant ionotropic glutamate receptors mediate thermosensation and hygrosensation in Drosophila. eLife, 5, e17879. doi:10.7554/eLife.17879

4. Drosophila melanogaster as a model organism to study nanotoxicity - Scientific Figure on ResearchGate. Available from: https://www.researchgate.net/figure/The-whole-life-cycle-of-the-fruit-fly-Drosophila-is-relatively-rapid-and-takes-only_fig1_264127592 [accessed 7 Aug, 2019]

Dowload poster

School of Neuroscience

Summer Undergraduate Research Fellowship 2019

COLLEGE OF SCIENCE
NEUROSCIENCE
VIRGINIA TECH™

School of Neuroscience at the College of Science (MC 0719)
Sandy Hall, Virginia Tech
210 Drillfield Dr.
Blacksburg, VA 24061
540-231-7995 | neuro@vt.edu
neuroscience.vt.edu